Accepted Manuscript

Record of Tethyan ocean closure and Indosinian collision along the Ailaoshan suture zone (SW China)

Huichuan Liu, Yuejun Wang, Peter A. Cawood, Weiming Fan, Yongfeng Cai, Xiaowan Xing

PII: S1342-937X(14)00008-2
DOI: doi: 10.1016/j.gr.2013.12.013
Reference: GR 1202

To appear in: *Gondwana Research*

Received date: 23 October 2013
Revised date: 18 December 2013
Accepted date: 21 December 2013

Please cite this article as: Liu, Huichuan, Wang, Yuejun, Cawood, Peter A., Fan, Weiming, Cai, Yongfeng, Xing, Xiaowan, Record of Tethyan ocean closure and Indosinian collision along the Ailaoshan suture zone (SW China), *Gondwana Research* (2014), doi: 10.1016/j.gr.2013.12.013

Record of Tethyan ocean closure and Indosinian collision along the Ailaoshan suture zone (SW China)

Huichuan Liu [1, 2, 3], Yuejun Wang [2, *], Peter A. Cawood [4, 5],

Weiming Fan [1], Yongfeng Cai [1, 3], Xiaowan Xing [1, 3]

[1] State Key Laboratory of Isotope Geochemistry, Guangzhou Institute of Geochemistry, Chinese Academy of Sciences, Guangzhou 510640, China

[2] Department of Earth Sciences, Sun Yat-Sen University, Guangzhou 510275, China

[3] University of Chinese Academy of Sciences, Beijing 100049, China

[4] Department of Earth Sciences, University of St Andrews, North Street, St Andrews KY169AL, UK

[5] Centre for Exploration Targeting, School of Earth and Environment, University of Western Australia, 35 Stirling Highway, Crawley, WA 6009, Australia

* Corresponding author
Current address:
Department of Earth Sciences,
Sun Yat-Sen University,
Guangzhou, 510275, China
Fax: 86-20-84111209, Tel: 86-20-84111209
Email: wangyuejun@mail.sysu.edu.cn

Abstract: Zircon U-Pb and Lu-Hf isotopic data along with whole-rock elemental and Sr-Nd isotopic analytical results for the Xin'anzhai and Tongtiange granitic plutons in the Ailaoshan suture zone record the transition from subduction to collision associated with the accretion of Indochina to Yangtze Blocks. The Xin'anzhai monzogranite yields zircon U-Pb age of 251.6 ± 2.0 Ma and $\varepsilon_{Hf}(t)$ values of -6.2 ~ -9.8. The Tongtiange leucogranite gives zircon U-Pb age of 247.5 ± 2.2 Ma and $\varepsilon_{Hf}(t)$ values ranging from -3.1 to -11.1. The Tongtiange leucogranites have lower MgO, Na_2O, CaO, FeOt and TiO_2 contents but higher A/CNK values than those of the Xin'anzhai monzogranites. The $\varepsilon_{Nd}(t)$ values for Xin'anzhai and Tongtiange plutons are in the range of -8.5 to -8.8 and -10.6 to -11.4, respectively, similar to those of the Ailaoshan metamorphic basement. The Tongtiange leucogranites are the product of dehydration melting of mica-rich metasedimentary rocks whereas the primary source of the Xin'anzhai monzogranites is probably Proterozoic gneiss with an addition of 35-45 % Proterozoic amphibolite. Our geochronological results, together with other published data, indicate the presence of Permo-Triassic magmatism associated with the Indosinian Orogeny along the Ailaoshan suture zone. This zone links with the Jinshajiang suture toward the northwest and the Song Ma-Hainan suture to the southeast. It is herein proposed that latest Permian convergent margin magmatism represented by the Xin'anzhai granitoid pluton (~252 Ma) terminated through the accretion of the Simao-Indochina to the South China Blocks, which marks the commencement of the Indosinian Orogeny resulting in the generation of the ~247 Ma Tongtiange S-type leucogranite.

Keywords: Paleotethyan evolution; Ailaoshan zone; Indosinian; Leucogranite; Syncollision

1. Introduction

Suture zones are major crustal discontinuities that record a history of ocean closure and continental collision (e.g., Dewey, 1977). They are marked by a succession of disrupted oceanic sedimentary and igneous rocks, often including slivers of ophiolite. They separate blocks of contrasting history and are zones of lithospheric weakness often resulting in a long and complex history of reactivation. Southeast Asia is cut by a series of suture zones that separate Gondwana-derived terranes at which record the transfer across the Tethys Ocean and accretion onto Asia during the late Paleozoic and Mesozoic (e.g., Cater et al., 2001; Metcalfe, 2002, 2006, 2011, 2013).

The Ailaoshan suture zone, the focus of this paper, separates the Yangtze Block of the South China Craton to the north from the Simao-Indochina Block to the south (Fig. 1a, Metcalfe, 2011, 2013). It is commonly accepted to link with the Jinshajiang suture toward the northwest and the Song Ma-Hainan suture to the southwest along strike extension. The zone incorporates a succession of Proterozoic and Paleozoic rocks, derived at least in part from the enclosing blocks, along with late Paleozoic to early Mesozoic ultramafic to silicic igneous rocks and associated sedimentary units (e.g., Zhong, 2000). Late Middle Triassic and younger rock-units (<240 Ma) unconformably overly the pre-Triassic packages both the bounding blocks and suture zone (e.g., Yunnan BGMR, 1990; Lepvrier et al., 2008). Cenozoic deformation associated with the India-Asia collision reactivated the Ailaoshan suture zone (e.g., Cao et al., 2012; Tang et al., 2013b) that is delineated by a series of faults, e.g., Red

River, Ailaoshan, Jiujia-Anding, Lixiangjiang and Tengtiaohe faults (Fig. 1b).

Previous works along the suture zone have focused on the ophiolitic assemblages (Xu and Castillo, 2004; Jian et al., 2009a, 2009b) and the Cenozoic deformation (Tapponnier et al., 1990; Cao et al., 2012; Tang et al., 2013b). In this paper we focus on the granitic rocks previously thought to be Proterozoic origin, which to date have received little attention (Yunnan BGMR, 1990) although work along the Jinshajiang and Song Ma-Hainan suture has established the presence of Permo-Triassic granites (e.g., Li et al., 2006; Zhu et al., 2011; Liu et al., 2012; Zi et al., 2012a, 2012b, 2012c, 2013). We present the geochronology and geochemistry of the granites along the Ailaoshan segment and then integrate these with available data along the entire Jinshajiang-Ailaoshan-Song Ma-Hainan suture zone to document the collisional history of the Simao-Indochina and Yangtze Blocks within a closure framework of the Tethyan Ocean.

2. Geological setting

The Jinshajiang-Ailaoshan-Song Ma-Hainan suture zone can be traced ~2900 km from Tibet to Hainan Island and is up to 100 km wide (Fig. 1a, Jian et al., 2009a; Metcalfe, 2011, 2013; Zhu et al., 2013; Zi et al., 2013). It is made up of four segments involving Jinshajiang, Ailaoshan, Song Ma and Hainan that record the effects of Cenozoic reactivation and further easterly extend into the South China Sea. It forms the western or southwestern boundary of the South China Craton, with the nature of the adjoining block varying along strike. The Ailaoshan segment separates the Yangtze Block of the South China Craton from the Simao-Indochina Block. The Yangtze Block

consists of Archean to Paleoproterozoic crystalline basement and Neoproterozoic to lower Paleozoic and upper Paleozoic marine assemblages (Gao et al., 1999; Cawood et al., 2013; Wang et al., 2013). The Simao Block consists of Mesoproterozoic metamorphic basement assemblage along with unconformity bound packages of lower Paleozoic metasedimentary rocks and middle Devonian conglomerates (Feng et al., 2000; Zhong, 2000). They are overlain in turn by a late Paleozoic sedimentary package containing late Devonian radiolarian bedded chert and Carboniferous to Permian shallow-marine limestone and sandstone (Yunnan BGMR, 1990; Metcalfe, 2002).

The Ailaoshan suture zone comprises structurally juxtaposed successions of variably metamorphosed Proterozoic and younger rock assemblages. The succession between the Red-River and Ailaoshan-Tengtiaohe faults, as shown in Fig. 1b, is dominated by a high-grade assemblage of paragneiss, granitic gneiss, hornblende-schist, marble and amphibolite with ages ranging from ~820 Ma to ~25 Ma (Lin et al., 2012; Qi et al., 2012; Liu et al., in press). In contrast, the region between the Ailaoshan and Lixianjiang faults (Fig. 1) contains greenschist-facies Paleozoic and Mesozoic strata, including ophiolitic fragments, greywacke, schist, chert and exotic limestone and associated volcanic rocks (Shen et al., 1998; Zhong, 2000). The ophiolitic fragments yielded the Devonian and Carboniferous ages (383-339 Ma, e.g., Jian et al., 2009b; Lai et al., in press). The main volcanic sequences in the shear zone are characterized by a Permian (287-265 Ma) basalt-andesite-dacite association that shows the geochemical affinity to arc magmatism in a supra-subduction setting (Fan et al., 2010).

A series of elongate granitic intrusions also occur within the Ailaoshan suture zone, especially in the region bounded by the Ailaoshan and Lixianjiang faults (Fig. 1b). They intrude Silurian to Permian strata (Yunnan BGMR, 1990) and both of these bodies, the Xin'anzhai and Tongtiange plutons, constitute the focus of this study. The Xin'anzhai pluton covers an area of ~450 km^2 and is unconformably overlain by the upper Triassic Gaoshanzhai Formation (Yunnan BGMR, 1990). It is a medium grained biotite monzogranite containing 30-40 % plagioclase, 25-35 % alkali feldspar, 25-30 % quartz and 3-7 % biotite, along with the accessory magnetite, zircon and apatite. The Tongtiange pluton within the central part of the Ailaoshan suture zone is strongly elongated and shows a parallel extension to the Ailaoshan fault (Fig. 1b). This pluton is a medium grained leucogranite containing 30-35 % plagioclase, 40-45 % alkali feldspar, 20-35 % quartz, 3-5 % biotite, 1-2 % muscovite and minor amounts of magnetite, zircon and apatite. Locations of samples for zircon geochronology and whole rock isotopic measurements are given in Table 1.

3. Analytical methods

Zircon mineral separates were prepared by conventional heavy liquid and magnetic techniques. Grains were mounted in epoxy, polished and coated with gold and then photographed in transmitted and reflected light. Their internal texture was examined using cathodoluminescence (CL) imaging at the Institute of Geology and Geophysics (IGG), Chinese Academy of Sciences (CAS), Beijing.

Zircon U-Pb ages and elements for samples HH-43A, HH-45A and ML-34G were analyzed using a Laser ICP-MS at the IGG CAS and those for sample ML-34A

at the State Key Laboratory of Continental Dynamics, Northwest University. The zircon standards CN92-2, 91500 and GJ were used to calibrate the U-Th-Pb ratios. The standard silicate glass NIST 610 was used to optimize the machine. The spot size for data collection was 30 μm. The errors for individual U-Pb analyses are presented with 1σ error and uncertainties in grouped ages are quoted at 95 % level (2σ). The age calculations and plots were made using Isoplot (version 3.0) (Ludwig, 2001). Further detailed descriptions of the instrumentation and analytical procedure for the LA-ICP-MS zircon U-Pb and trace element technique are similar to those described by Yuan et al. (2004). Zircon Hf isotopic analysis was carried out using a Geolas-193 laser-ablation microprobe, attached to a Neptune multi-collector ICP-MS at the IGG CAS. All of the settings yielded a signal intensity of ~10 Vat ^{180}Hf for the standard zircon 91500 with a recommended $^{176}Hf/^{177}Hf$ ratio of 0.282293 ± 28 (Wu et al., 2006). Data were normalized to $^{176}Hf/^{177}Hf$=0.7325, using exponential correction for mass bias. The mean β_{Yb} value was applied for the isobaric interference correction of ^{176}Yb on ^{176}Hf in the same spot. The ratio of $^{176}Yb/^{172}Yb$ (0.5887) was also applied for the Yb correction.

Whole rock samples for geochemistry were crushed to 200-mesh using an agate mill for elemental and Sr-Nd isotopic analyses. The major oxides were analyzed by a wavelength X-ray fluorescence spectrometry at the State Key Laboratory of Isotope Geochemistry, Guangzhou Institute of Geochemistry (GIG), Chinese Academy of Sciences (CAS). Trace element analyses were performed at the GIG CAS by a Perkin-Elmer Sciex ELAN 6000 ICP-MS. Detailed sample preparation and analytical

procedure followed Li et al. (2002). Sr, Nd isotopic analyses were carried out at the GIG CAS on a Neptune Plus (Thermo Fisher Scientific, MA, USA) multi-collection mass spectrometry equipped with nine Faraday cup collectors and eight ion counters. Details analytical methods are presented by Yang et al. (2006). Normalizing factors used to correct the mass fractionation of Sr and Nd during the measurements were $^{86}Sr/^{88}Sr = 0.1194$ and $^{146}Nd/^{144}Nd = 0.7219$ (Yang et al., 2005, 2007).

4. Zircon U-Pb and Lu-Hf systematics

Four representative samples, two biotite monzogranites from the Xin'anzhai pluton (HH-43A and HH-45B) and two leucogranites from the Tongtiange pluton (ML-34A and ML-34G) were collected for zircon isotopic analysis (Supplementary Data Table 1). Zircon grains for in-situ U-Pb and Lu-Hf isotopic analyses were mostly euhedral, transparent to colorless, and stubby to elongate in shape with the lengths of 100-200 μm and widths of 40-90 μm (Figs. 2a and b). Backscatter electron (BSE) and CL images of all grains display well-preserved euhedral growth zones, with unperturbed oscillatory zoning, typical of igneous zircon (e.g., Hanchar and Miller, 1993).

4.1. Zircon U-Pb geochronology

Zircon U-Pb dating results are listed in the Supplementary Data Table 1 and presented on concordia plots in Figs. 2c-f. U and Th concentrations for all analyzed grains range from 87 to 1225 ppm and 508 to 5528 ppm, respectively, with Th/U ratios of 0.10 to 0.69, consistent with an igneous origin. The $^{206}Pb/^{238}U$ weighted mean ages were used to determine crystallization ages.

Xin'anzhai pluton: The majority of analyzed 22 grains from sample HH-43A have $^{206}Pb/^{238}U$ apparent ages ranging from 259.0 ± 6.6 Ma to 246.2 ± 6.8 Ma and form a coherent group with a weighted mean age of 251.9 ± 1.4 Ma (MSWD = 0.84, Fig. 2c). Spots HH-43A-6, -10 and -20 give $^{206}Pb/^{238}U$ apparent ages of 825.7 ± 20.5 Ma, 634.8 ± 16.5 Ma and 496.9 ± 12.7 Ma, respectively, representative of inherited grains. For sample HH-45B, twenty-two of 25 analyses yield $^{206}Pb/^{238}U$ apparent ages between 258.3 ± 6.9 Ma and 246.8 ± 7.8 Ma and give a weighted mean age of 251.2 ± 1.4 Ma (MSWD = 0.90, Fig. 2e). Three analyses on 3 spots yield $^{206}Pb/^{238}U$ ages of 454.1 ± 11.6 Ma (HH-45B-11), 746.4 ± 18.9 Ma (HH-45B-13) and 384.7 ± 10.0 Ma (HH-45B-17), interpreted as the result of inheritance. Combining the 44 zircon analyses of the two samples, it is given for a $^{206}Pb/^{238}U$ mean age of 251.6 ± 2.0 Ma (MSWD = 0.21), which is taken as the crystallization age of the Xin'anzhai pluton.

Tongtiange pluton: For sample ML-34A, 22 analyses form a coherent group yielding a $^{206}Pb/^{238}U$ weighted mean age of 247.3 ± 3.1 Ma (MSWD = 0.20, Fig. 2d). Six grains give Proterozoic (1297-799 Ma) and Cambrian (537-501 Ma) ages that are interpreted as representative of the inherited material. Fourteen of 23 grains from ML-34G form a cluster with the weighted mean age of 247.7 ± 3.0 Ma (MSWD = 0.37, Fig. 2f), representing the crystallization age of the Tongtiange pluton. Another seven grains give older $^{206}Pb/^{238}U$ apparent ages ranging from 838 Ma to 412 Ma, inferred to represent inherited material. The 36 zircon analyses for the two samples give a weighted mean $^{206}Pb/^{238}U$ age of 247.5 ± 2.2 Ma (MSWD=0.26), which is taken as the crystallization age of the Tongtiange pluton.

4.2. Zircon in-situ Lu-Hf isotopes

Zircon Lu-Hf isotopic results for the dated samples are listed in Supplementary Data Table 1 and shown on Fig. 3. Initial Hf isotopic ratios are recalculated to the crystallization ages, using the ^{176}Lu-^{176}Hf decay constant reported by Soderlund et al. (2004). ^{176}Lu/^{177}Hf ratios of most zircons are less than 0.003 (Supplementary Data Table 1), indicating a low radiogenic growth of ^{176}Hf. Two-stage model ages (T_{DM2}) are calculated for the source rock of magma by assuming a mean ^{176}Lu/^{177}Hf value of 0.015 for the average continental crust (Griffin et al., 2002).

Xin'anzhai pluton: Three inherited zircons from HH-43A have $\varepsilon_{Hf}(t)$ values +4.3, -4.8 and -9.3. Twenty-two grains used to constrain the crystallization age of the pluton exhibit uniform Hf isotopic ratios, with $\varepsilon_{Hf}(t)$ values ranging from -9.8 to -6.2. The corresponding T_{DM2} ages are in the range of 1.90-1.67 Ga. For HH-45B, the twenty-two grains with the crystallization age show $\varepsilon_{Hf}(t)$ values ranging from -11.1 to -3.1 and T_{DM2} ages from 2.0 Ga to 1.47 Ga. The other three inherited zircons from this sample show $\varepsilon_{Hf}(t)$ values -8.5, -6.7 and +2.3, respectively.

Tongtiange pluton: Grains with early Triassic crystallization ages from the pluton have negative $\varepsilon_{Hf}(t)$ values ranging from -16.6 to -3.2 for sample ML-34A and -11.9 to -3.4 for ML-34G and the corresponding T_{DM2} ages are in the range of 2.32-1.48 Ga and 2.03-1.49 Ga, respectively.

5. Whole-rock geochemical results

The whole-rock major oxides and trace elemental data for the analyzed samples are listed in Table 2. Samples from the Xin'anzhai pluton exhibit low SiO_2, high MgO,

Na_2O and CaO contents (Fig. 4) and are weakly peraluminous, with A/CNK [molar $Al_2O_3/(CaO+Na_2O+K_2O)$] ranging from 1.03 to 1.12. CIPW-normative calculations show 27-30 vol. % quartz, 21-29 vol. % orthoclase, 25-28 vol. % albite, 6-14 vol. % anorthite and 0.9-2.0 vol. % corundum. These signatures suggest a transition from S-type to I-type granite (Chappell, 1999). On Harker variation diagrams, SiO_2 correlates negatively with Al_2O_3, MgO, CaO, FeOt and TiO_2 (Figs. 4c-f and h) and a similar correlation is also shown by Sr, Ba, Eu, Zr and La (Figs. 5a-d and f).

Samples from the Tongtiange pluton have a modal composition containing 43-56 vol. % quartz, 20-34 vol. % orthoclase, 9-18 vol. % albite, and 0-0.5 vol. % anorthite. They display high A/CNK values ranging from 1.29 to 1.87 (Fig. 4a). In comparisons with those of the Xin'anzhai pluton, the Tongtiange samples exhibit lower FeOt, Na_2O, TiO_2 and P_2O_5 but higher K_2O contents (Fig. 4). Corundum content is more than 1.0 vol. %. These features are consistent with S-type granites (Clemens, 2003). On Harker variation diagrams, most major element oxides and trace elements do not display any significant correlations with SiO_2 (Figs. 4 and 5).

Samples from the Xin'anzhai and Tongtiange plutons show similar chondrite-normalized REE patterns (Fig. 6a) in spite of the distinct total REE contents, with LREE enrichment and moderate LREE/HREE fractionation. The Xin'anzhai monzogranites have total REE contents of 124-211 ppm with (La/Yb)n=5.90-12.73, (Gd/Yb)n=1.49-1.95 and Eu/Eu*=0.47-0.63. The Tongtiange leucogranites have lower total REE contents (45-112 ppm) and more significant negative Eu anomalies (Eu/Eu* =0.16-0.45). Their (La/Yb)n ratios range from 2.96 to 10.27 and (Gd/Yb)n from 0.90

to 1.89. On the multi-elemental primitive mantle-normalized spider diagram (Fig. 6b), these samples are characterized by strong depletions in Ba, Nb-Ta, Sr and Ti and enrichment in Th and U.

The initial isotopic ratios of the analyzed samples were recalculated to their crystallization age of 250 Ma. The Xin'anzhai monzogranites are characterized by initial $^{87}Sr/^{86}Sr$ ratios of 0.71493 to 0.71603 and $\varepsilon_{Nd}(t)$ values of -8.5 to -8.8 (Fig. 7). The Tongtiange granites have high $^{87}Rb/^{86}Sr$ ratios (14.25 to 29.43) and the Rb-error-induced uncertainties in initial Sr isotopic errors are significant (Jahn et al., 2000). The Tongtiange granites, relative to the Xin'anzhai monzogranites, display more enriched Nd isotopic compositions with $\varepsilon_{Nd}(t)$ values of -10.6 to -11.4 (Fig. 7b).

6. Discussion

6.1. Petrogenesis

The Tongtiange and Xin'anzhai plutons show contrasting geochemical signatures, indicative of distinct magma evolution or petrogenesis. Samples from the Tongtiange pluton display random variations of major element oxides and trace elements (Figs. 4a-f and 5), indicating that crystal fractionation played an insignificant role during magma evolution. Pronouncedly negative Ba, Eu and Sr and positive Rb anomalies suggest the presence of residual plagioclase and K-feldspar in the source region (Figs. 6a-b; Rapp et al., 2003). The strongly negative correlation between Rb/Sr and Ba (Fig. 9) is consistent with dehydration melting of mica-bearing metasedimentary rocks with alkali feldspar as a residual phase (Harris and Inger, 1992; Zhang et al., 2004), resembling to that of the High Himalayan

leucogranites (Zhang et al., 2004; Streule et al., 2010). The Tongtiange samples are strongly peraluminous granites, suggesting an origination of (1) aluminous-rich meta-sedimentary rocks, (2) amphibolites under H_2O-rich conditions (Ellis and Thompson, 1986), or (3) fractionation of aluminous-poor magma (Zen, 1986). However, the products from either case (2) or (3) are usually characterized by Na- and Sr-enrichment (Ellis and Thompson, 1986; Zen, 1986), which contrasts to the results from the Tongtiange S-type granites (Figs. 4g and 5a). These S-type granites have the highest SiO_2 and lowest FeOt, CaO, MgO and TiO_2 contents among the reported igneous rocks along the Ailaoshan shear zone, indicating that they are unlikely to be derived by mixing between mantle-derived mafic and crust-derived felsic magmas. Thus, it is most likely that these granites originated from a meta-sedimentary source. This is further supported by the following observations. (1) The Tongtiange samples fall into the fields of partial melt of metapelites and metagrewackes (Figs. 8a-f). (2) They show lower Ce/Pb and Nb/U ratios than upper continental crust (Figs. 8g-h). (3) The samples have significant negative Sr and Ti anomalies, and negative $\varepsilon_{Nd}(t)$ values (-11.4 to -10.6), and are geochemically similar to mid-Tertiary granites in the South Colorado Minerla Belt that are interpreted as the anatexic product of the metasedimentary source (Anthony, 2005). (4) The presence of the Proterozoic inherited zircons and the Proterozoic zircon Hf model ages (T_{DM2} = 2.32-1.48 Ga), similar to the Ailaoshan Proterozoic gneisses with Nd model ages of 1.84-1.65 Ga, indicate the potential source for the Tongtiange S-type granites. In summary, the Tongtiangge granites are product of the dehydration

melting of mica-rich meta-sedimentary rocks.

The linear trends of major oxides and trace elements for the Xin'anzhai granitic samples (Figs. 4 and 5) suggest that crystal fractionation played an important role in magma evolution. The decreases of Al_2O_3, CaO, FeOt and MgO with increasing SiO_2 illustrate the importance of fractional crystallization of plagioclase, K-feldspar and biotite. The distinctly negative Sr, Ba and Eu anomalies (Fig. 6) and the decreases of Sr, Ba and Eu with increasing SiO_2 (Figs. 5a-c) are consistent with the removal of plagioclase and K-feldspar during magma evolution. Fractionation of Ti-Fe oxides is indicated by strongly negative Ti anomalies (Fig. 6a) and the decreases of TiO_2 and FeOt (Figs. 4g and 4h) with increasing SiO_2. The Xin'anzhai granites are mildly peraluminous with a narrow range of A/CNK from 1.03 to 1.12 and have higher Na and Sr contents in comparison with the Tongtiange S-type granites (Figs. 4a, 4g and 5a). The Xin'anzhai granites exhibit low Rb/Sr and Al_2O_3/TiO_2 ratios but high Sr/Ba and CaO/Na_2O ratios, indicating a mixed source of meta-sedimentary with meta-igneous rocks (Figs. 8a and c; e.g., Chappell and White, 1992; Jung et al., 2003). Other evidence for a two-component mixing origin for the Xin'anzhai granites include: (1) MgO + FeO + TiO_2 decrease with increasing SiO_2 (Fig. 4b); (2) the Xin'anzhai samples fall in the overlapping field of partial melts of greywackes and amphibolites (Figs. 8b-f); and (3) mafic enclaves in the pluton (Yunnan BGMR, 1990) may be representative of the mafic end-member component. Experimental studies have demonstrated that partial melting of basaltic rocks can produce intermediate to silicic melts leaving a granulite residue at 8-12 kbar or an eclogite residue at 12-32 kbar

(Rapp and Watson, 1995; Chen and Arakawa, 2005). A number of factors suggest that the formation age of the mafic source was considerably older than the timing of granite emplacement. These factors include that: (1) the Xin'anzhai granites have lower Ce/Pb and Nb/U ratios than the upper continental crust (Figs. 8g-h); (2) zircon $\varepsilon_{Hf}(t)$ isotopic compositions are characterized by the negative values (-11.1 to -3.1) and Proterozoic (2.0-1.5 Ga) Hf model ages. Consequently, the formation of the Xin'anzhai granite is attributed to melting of an ancient source consisting of interlayered meta-basaltic and meta-sedimentary rocks. Such a lithologic assemblage can be commonly observed within the Ailaoshan shear zone (Yunnan BGMR, 1990). Mixing calculations show that the primary source of the Xin'anzhai granites is probably constituted by the addition of 35-45 % Proterozoic amphibolites with Proterozoic pelitic gneisses (Fig. 7a).

Experimental data has demonstrated that biotite, muscovite and feldspar in paragneiss will breakdown when the temperature is higher than 800-850 ℃ (Thompson and Connolly, 1995), but dehydration melting of amphibolites requires much higher temperatures (>1000℃, Rapp and Watson, 1995). Numerical modeling by Ellis and Thompson (1986) and Wang et al. (2007) reveals that widespread anatexis occur at mid- or lower crustal levels when the crust is tectonically thickened 1.5 to 2 times. Furthermore, a 50 % increase of heat production in the tectonically thickened crust could raise the temperature at its base by 150-200°C. Indosinian pelitic granulite in the Ailaoshan suture zone showed the peak metamorphic temperature of 850-919°C (Qi et al., 2012). Thus, the thermal budget provided by

radioactive decay and crustal thickening would be sufficient to achieve the high-grade metamorphic conditions and to induce partial melting of the Neoproterozoic gneisses at middle or lower crustal depths. However, such conditions are insufficient to trigger the partial melting of the Neoproterozoic amphibolites at lower crust levels without additional heat input from the mantle processes.

6.2. Record of Indosinian Orogenesis along the Ailaoshan zone and environs

The concept of the Indosinian Orogeny was originally established on the basis of the unconformity between Upper Triassic red-beds and deformed Middle Triassic and older metamorphic rocks in northern Vietnam (e.g. Deprat, 1914; Lepvrier et al., 2008). Early Indosinian age data have, until recently, been relatively limited in the vicinity of the Ailaoshan suture zone with the exception of the Lvchun rhyolite (247.3 ± 1.8 Ma) of the Gaoshanzhai Formation (Liu et al., 2011), which constitutes part of the post-unconformity Indosinian cover succession. Our data show that the Xin'anzhai pluton has a zircon U-Pb age of 251.6 ± 2.0 Ma and that the Tongtiange pluton is dated at 247.5 ± 2.2 Ma. These ages are consistent with field relations that the plutons intrude Silurian strata and that the Xin'anzhai pluton is unconformably overlain by the Gaoshangzhai Formation (YunnanBGMR, 1990).

A compilation of age-data shows that early Indosinian magmatic activity is widespread in the vicinity of the Jinshajiang, Song Ma and Hainan zones (Fig. 10). In general, the igneous rocks with the crystallization age of >247 Ma are mainly composed of diorite, granodiorite and monogranite and exhibit similar geochemical signatures to the Xin'anzhai granites. These bodies include the Baimaxueshan pluton

(254-248 Ma) along the Jinshajiang suture zone (Zi et al., 2012a), the Muong Lay (248 Ma) and Phia Bioc (245-248 Ma) plutons of the Song Ma zone (Liu et al., 2012; Roger et al., 2012), and the Xinqing, Nankun, Beida and Ledong plutons on Hainan island, which give zircon U-Pb ages in the range ~257-253 Ma (Zhang et al. 2012; Wen, 2013). In contrast younger igneous activities (<247 Ma) along the suture zones, e.g., high-Si rhyolites in the Renzhixueshan (247 Ma, Wang et al., 2011), Pantiange (247-246 Ma, Zi et al., 2012c) and Gaoshanzhai (247 Ma, Liu et al., 2011) Formations and the Pingzhang granite (244 Ma, Lai et al., in press), geochemically resemble the high silica, peraluminous Tongtiange granites. Late Indosinian granitoid plutons were also found along these zones. For example in the Hainan and Song Ma zone, the Dien Bien granodiorite and monzonite, the Panyang and Xinlong syenogranites were dated at 229-202 Ma and ~234 Ma, respectively (Liu et al., 2012; Tang et al., 2013a; Wen, 2013). The Ludian, Jiaren, Gongka and Yangla granodiorite and monzogranite plutons in the Jinshajiang zone yield U-Pb ages of 234-214 Ma with their main rocks types of granodiorites and monzogranites (Gao et al., 2010; Zhu et al., 2011; Zi et al., 2013). The rhyolite and rhyodacite in the upper units of the Cuiyibi Formation were dated at 242-239 Ma (Zi et al., 2012c). Furthermore, the extrusive components of this magmatic activity are unconformable on older deformed units and thus tightly constrain the tectonothermal activity to the Early Triassic at ~247 Ma (Fig. 10).

Data of the metamorphic rocks from either within the suture zone or the adjoining Yangtze and Simao-Indochina Blocks also suggest orogenesis occurring during earliest Triassic period. The syn-kinematic hornblende, biotite and muscovite

along a series of northwest to west-northwest trending dextral strike-slip and transpression shear zones in the vicinity of Ailaoshan, Hainan and North Vietnam yield $^{40}Ar/^{39}Ar$ plateau ages ranging from 250 to 240 Ma (Fig. 10, e.g., Lepvrier et al., 1997; Lepvrier et al., 2004; Zhang et al., 2011). Metamorphic zircons in high-grade rocks in northern Vietnam give the ages of 250-245 Ma (e.g., Carter et al., 2001; Nam et al., 2001; Roger et al., 2007). A monazite U-Pb age of 243 ± 4 Ma is given by an eclogite in the Song Ma zone (Nakano et al., 2010), suggesting a significant crustal thickening during the Triassic. Similarly, it is discovered for the high-pressure pelitic granulite along the Ailaoshan suture zone being correlated with the high-grade metamorphic rocks along Song Ma zone (Qi et al., 2012).

6.3. Tectonic implication

Figure 11 presents a compilation of Paleozoic to early Mesozoic age data for igneous rock units entrained along the Jinshajiang-Ailaoshan-Song Ma-Hainan suture zone. In combination with the geological and geochemical data for the nature of the rock associations, three phases of igneous activity can be recognized: 1) an early phase at ~390-305 Ma, which is marked by ophiolitic rock units that have been considered to indicate a back-arc basin or ocean setting (e.g., Wang et al., 2000; Zhong, 2000; Jian et al., 2009b; Lai et al. in press); 2) mafic to felsic magmatism extending from 305 to 248 Ma that have formed in a supra-subduction zone (e.g., Peng et al., 2008; Jian et al., 2009b; Fan et al., 2010; Liu et al., 2011; Li et al., 2012; Liu et al., 2012; Zi et al., 2012a, 2012b); and 3) post-247 Ma high-silica peraluminous igneous rocks that mark the onset of the Indosinian Orogeny (Liu et al., 2011; Wang

et al., 2011; Zi et al., 2012c, 2013).

Ages of the end Carboniferous to earliest Mesozoic supra-subduction zone activity (305-248 Ma) can be internally divided into three pulses at approximately ~305-280 Ma, 270-265 Ma and 255-248 Ma (Fig. 11). The third pulse includes the Xin'anzhai pluton. The petrographical and geochemical characteristics of the pluton are similar to the Baimaxueshan I-type pluton that constitutes part of the volcano-plutonic arc created by westward-directed subduction (e.g., Zi et al., 2012a). In addition, the 249 Ma Maoheshan basalts in the Ailaoshan suture zone are considered to be derived from a mantle wedge source in an arc setting (Liu et al., 2011). Thus, the Xin'anzhai pluton is considered to be a latest Permian expression of arc magmatism in SW Yunnan. Furthermore, the underplating of asthenospheric mantle associated with the supra-subduction zone setting provides a likely heat source for the melting of the Neoproterozoic amphibolites and interlayered meta-sedimentary rocks to generate the magma of the Xin'anzhai pluton.

Our data show that the Tongtiange leucogranite formed at ~247 Ma, slightly younger than that of the Xin'anzhai granite. The pluton is geochemically similar to the time-equivalent high-Si rhyolite of the Gaoshanzhai, Renzhixueshan and Pantiange Formations that are interpreted as the product of syncollisional melting during assembly of the Yangtze and Simao-Indochina blocks (e.g., Liu et al., 2011; Wang et al., 2011; Zi et al., 2012c). Indosinian pelitic granulites in the Ailaoshan suture zone reveal the temperature of peak metamorphism up to 850-919°C (Qi et al., 2012). Such temperature corresponds to the breakdown temperature of biotite,

muscovite and feldspar in gneiss (Thompson and Connolly, 1995). Such conditions of the temperature in the syncollisional setting in response to the assembly of the Yangtze and Simao-Indochina blocks could result into the dehydration melting of mica-rich meta-sedimentary source to produce the Tongtiange leucogranite magma.

In summary, convergent margin magmatism was preserved along the Jinshajiang-Ailaoshan-Song Ma-Hainan suture zone and terminated at around 247 Ma, which is represented in the study area by the 252 Ma Xin'anzhai pluton. Termination of convergent plate activity was immediately followed by regional compressive deformation and high-grade metamorphism. The compression regime marks the commencement of the Indosinian Orogeny associated with assembly of the Yangtze and Simao-Indochina blocks and resulted in the generation of the ~247 Ma Tongtiange S-type leucogranite.

Acknowledgements

We acknowledge F Guo, T-P Peng, J-W Zi and X-P Xia for their help during the fieldwork. We are grateful to Y Liu, L Qi and H Zhang for their assistance during geochemical analyses and LA-ICPMS dating. We thank Ian Metcalfe and an anonymous reviewer for their thorough, critical and constructive reviews and comments, and Prof. W-J Xiao for his editorial advice. This study was jointly supported by China Natural Science Foundation (41190073, 41372198 and 40825009), National Basic Research Program of China (2014CB440901) and State Key Laboratory of Ore Deport Geochemistry, CAS (201301).

References

Anthony, E.Y., 2005. Source regions of granites and their links to tectonic environment: examples from the western United States. Lithos 80, 61-74.

Cao, S.Y., Liu, J.L., Leiss, B., Vollbrecht, A., Genser, J., Neubauer, F., Zhao, C.Q., 2012. Initiation of left-lateral deformation along the Ailao Shan-Red River shear zone: new microstructural, textural, and geochronological constraints from the Diancang Shan metamorphic massif, SW Yunnan, China. International Geology Review 54, 348-367.

Carter, A., Roques, D., Bristow, C., Kinny, P., 2001. Understanding Mesozoic accretion in Southeast Asia: significance of Triassic thermotectonism (Indosinian orogeny) in Vietnam. Geology 29, 211-214.

Cawood, P.A., Wang, Y.J., Xu, Y.J., Zhao, G.C., 2013. Locating South China in Rodinia and Gondwana: a fragment of Greater India lithosphere? Geology 41, 903-906.

Chappell, B.W., 1999. Aluminium saturation in I- and S-type granites and the characterization of fractionated haplogranites. Lithos 46, 535-551.

Chappell, B.W., White, A.J.R., 1992. I-Type and S-type granites in the Lachlan fold belt. Transactions of the Royal Society of Edinburgh-Earth Sciences 83, 1-26.

Chen, B., Arakawa, Y., 2005. Elemental and Nd-Sr isotopic geochemistry of granitoids from the West Junggar foldbelt (NW China), with implications for Phanerozoic continental growth. Geochimica et Cosmochimica Acta 69, 1307-1320.

Clemens, J.D., 2003. S-type granitic magmas: petrogenetic issues, models and evidence. Earth-Science Reviews 61, 1-18.

Deprat, J., 1914. Etude des plissements et des zones décrasement de la moyenne et de la basse Rivière Noire. Mèmoire du Service Géologique Indochine 3-4, 1-59.

Dewey, J.F., 1977. Suture Zone Complexities: Review. Tectonophysics 40, 53-67.

Ellis, D.J., Thompson, A.B., 1986. Subsolidus and partial melting reactions in the quartz-excess $CaO+MgO+Al_2O_3+SiO_2+H_2O$ system under water-excess and water-deficient conditions to 10 kb - some implications for the origin of peraluminous melts from mafic rocks. Journal of Petrology 27, 91-121.

Fan, W.M., Wang, Y.J., Zhang, A.M., Zhang, F.F., Zhang, Y.Z., 2010. Permian arc-back-arc basin development along the Ailaoshan tectonic zone: geochemical, isotopic and geochronological evidence from the Mojiang volcanic rocks, Southwest China. Lithos 119, 553-568.

Feng, Q.L., Zhang, Z.F., Liu, B.P., Shen, S.Y., 2000. Radiolarian Fauna from the Longdonghe Formation at the western margin of the Simao massif and its geologoical significance. Journal of Stratigraphy 24, 126-128 (in Chinese with English abstract).

Gao, R., Xiao, L., He, Q., Yuan, J., Ni, P.Z., Du, J.X., 2010. Geochronology, geochemistry and petrogenesis of granites in Weixi-Deqin, West Yunnan. Earth Science-Journal of China University of Geosciences 35, 186-200 (in Chinese with English abstract).

Gao, S., Ling, W.L., Qiu, Y.M., Lian, Z., Hartmann, G., Simon, K., 1999. Contrasting

geochemical and Sm-Nd isotopic compositions of Archean metasediments from the Kongling high-grade terrain of the Yangtze craton: evidence for cratonic evolution and redistribution of REE during crustal anatexis. Geochimica Et Cosmochimica Acta 63, 2071-2088.

Gradstein, J.G.O., Smith, A.G., Bleeker, W., Lourens, L.J., 2004. A new geological timescale, with special reference to Precambrian and Neogene. Episodes 27, 83-99.

Griffin, W.L., Wang, X., Jackson, S.E., Pearson, N.J., O'Reilly, S.Y., Xu, X.S., Zhou, X.M., 2002. Zircon chemistry and magma mixing, SE China: In-situ analysis of Hf isotopes, Tonglu and Pingtan igneous complexes. Lithos 61, 237-269.

Hanchar, J.M., Miller, C.F., 1993. Zircon zonation patterns as revealed by Cathodoluminescence and Backscattered electron images: implications for interpretation of complex crustal histories. Chemical Geology 110, 1-13.

Harris, N.B.W., Inger, S., 1992. Trace element modeling of pelite-derived granites. Contributions to Mineralogy and Petrology 110, 46-56.

Inger, S., Harris, N., 1993. Geochemical Constraints on leucogranite magmatism in the Langtang Valley, Nepal Himalaya. Journal of Petrology 34, 345-368.

Jahn, B.M., Wu, F.Y., Chen, B., 2000. Granitoids of the Central Asian Orogenic Belt and continental growth in the Phanerozoic. Transactions of the Royal Society of Edinburgh-Earth Sciences 91, 181-193.

Jian, P., Liu, D.Y., Kroner, A., Zhang, Q., Wang, Y.Z., Sun, X.M., Zhang, W., 2009a. Devonian to Permian plate tectonic cycle of the Paleo-Tethys Orogen in southwest China (I): Geochemistry of ophiolites, arc/back-arc assemblages and within-plate igneous rocks. Lithos 113, 748-766.

Jian, P., Liu, D.Y., Kroner, A., Zhang, Q., Wang, Y.Z., Sun, X.M., Zhang, W., 2009b. Devonian to Permian plate tectonic cycle of the Paleo-Tethys Orogen in southwest China (II): Insights from zircon ages of ophiolites, arc/back-arc assemblages and within-plate igneous rocks and generation of the Emeishan CFB Province. Lithos 113, 767-784.

Jian, P., Liu, D.Y., Wang, X.F., 2003. SHRIMP dating of Baimaxueshan and Ludian granitoid batholiths in northwestern Yunnan Province and its geological implications. Acta Geoscientia Sinica 24, 337-342 (in Chinese with English abstract).

Jung, S., Mezger, K., Hoernes, S., 2003. Petrology of basement-dominated terranes. II. Contrasting isotopic (Sr, Nd, Pb and O) signatures of basement-derived granites and constraints on the source region of granite (Damara orogen, Namibia). Chemical Geology 199, 1-28.

Lai, C.K., Meffre, S., Crawford, A.J., Zaw, K., Halpin, J.A., Xue, C.D., Salam, A., Manaka, T., in press. Nature of the Paleozoic central Ailaoshan mélange: opening and closure of the Ailaoshan-Song Ma Paleotethys branch. Gondwana Research.

Lepvrier, C., Maluski, H., Van Tich, V., Leyreloup, A., Thi, P.T., Van Vuong, N., 2004. The Early Triassic Indosinian orogeny in Vietnam (Truong Son Belt and Kontum Massif): implications for the geodynamic evolution of Indochina. Tectonophysics 393, 87-118.

Lepvrier, C., Maluski, H., Van Vuong, N., Rogues, D., Axente, V., Rangin, C., 1997. Indosinian NW-trending shear zones within the Truong Son belt (Vietnam) Ar^{40}-Ar^{39} Triassic ages and Cretaceous to Cenozoic overprints. Tectonophysics 283, 105-127.

Lepvrier, C., Van, V.N., Maluski, H., Thi, P.T., Van, V.T., 2008. Indosinian tectonics in Vietnam. Comptes Rendus Geoscience 340, 94-111.

Li, G.Z., Li, C.S., Ripley, E.M., Kamo, S., Su, S.G., 2012. Geochronology, petrology and geochemistry of the Nanlinshan and Banpo mafic-ultramafic intrusions: implications for subduction initiation in the eastern Paleo-Tethys. Contributions to Mineralogy and Petrology 164, 773-788.

Li, X.H., Li, Z.X., Li, W.X., Wang, Y.J., 2006. Initiation of the Indosinian Orogeny in South China: Evidence for a Permian magmatic arc on Hainan Island. Journal of Geology 114, 341-353.

Li, X.H., Li, Z.X., Zhou, H.W., Liu, Y., Kinny, P.D., 2002. U-Pb zircon geochronology, geochemistry and Nd isotopic study of Neoproterozoic bimodal volcanic rocks in the Kangdian Rift of South China: implications for the initial rifting of Rodinia. Precambrian Research 113, 135-154.

Lin, T.H., Chung, S.L., Chiu, H.Y., Wu, F.Y., Yeh, M.W., Searle, M.P., Iizuka, Y., 2012. Zircon U-Pb and Hf isotope constraints from the Ailao Shan-Red River shear zone on the tectonic and crustal evolution of southwestern China. Chemical Geology 291, 23-37.

Liu, C., Deng, J.F., Liu, J.L., Shi, Y.L., 2011. Characteristics of volcanic rocks from Late Permian to Early Traissic in Ailaoshan tectono-magmatic belt and implications for tectonic settings. Acta Petrologica Sinica 27, 3590-3602 (in Chinese with English abstract).

Liu, C., Deng, J.F., Liu, J.L., Su, S.G., Chen, Y., Kong, W.Q., 2010. Ailaoshan ophiolite belt, Yunnan Province, southwestern China: SSZ type or MORS type? Geochimica et Cosmochimica Acta 74, A609.

Liu, H.C., Wang, Y.J., Fan, W.M., Zi, J.W., Cai, Y.F., Xing, X.W., in press. Petrogenesis and tectonic implications of Late-Triassic high εNd(t)-εHf(t) granites in the Ailaoshan tectonic zone (SW China). Science China-Earth Sciences.

Liu, J.L., Tran, M.D., Tang, Y., Nguyen, Q.L., Tran, T.H., Wu, W.B., Chen, J.F., Zhang, Z.C., Zhao, Z.D., 2012. Permo-Triassic granitoids in the northern part of the Truong Son belt, NW Vietnam: geochronology, geochemistry and tectonic implications. Gondwana Research 22, 628-644.

Ludwig, K.R., 2001. Sqiud 1.02: A User Manual. Berkeley: Berkeley Geochronological Center Special Publication, 1-219.

Metcalfe, I., 2002. Permian tectonic framework and palaeogeography of SE Asia. Journal of Asian Earth Sciences 20, 551-566.

Metcalfe, I., 2006. Paleozoic and Mesozoic tectonic evolution and palaeogeography of East Asian crustal fragments: The Korean Peninsula in context. Gondwana Research 9, 24-46.

Metcalfe, I., 2011. Tectonic framework and Phanerozoic evolution of Sundaland. Gondwana

Research 19, 3-21.

Metcalfe, I., 2013. Gondwana dispersion and Asian accretion: Tectonic and palaeogeographic evolution of eastern Tethys. Journal of Asian Earth Sciences 66, 1-33.

Nakano, N., Osanai, Y., Minh, N.T., Miyamoto, T., Hayasaka, Y., Owada, M., 2008. Discovery of high-pressure granulite-facies metamorphism in northern Vietnam: cnstraints on the Permo-Triassic Indochinese continental collision tectonics. Comptes Rendus Geoscience 340, 127-138.

Nakano, N., Osanai, Y., Sajeev, K., Hayasaka, Y., Miyamoto, T., Minh, N.T., Owada, M., Windley, B., 2010. Triassic eclogite from northern Vietnam: inferences and geological significance. Journal of Metamorphic Geology 28, 59-76.

Nam, T.N., Sano, Y., Terada, K., Toriumi, M., Van Quynh, P., Dung, L.T., 2001. First SHRIMP U-Pb zircon dating of granulites from the Kontum massif (Vietnam) and tectonothermal implications. Journal of Asian Earth Sciences 19, 77-84.

Patiňo-Douce, A.E., 1999. What do experiments tell us about the relative contributions of crust and mantle to the origin of granitic magmas. Geological Society London, Special Publications 168, 55-75.

Patiňo-Douce, A.E., Harris, N., 1998. Experimental constraints on Himalayan anatexis. Journal of Petrology 39, 689-710.

Peng, T.P., Wang, Y.J., Zhao, G.C., Fan, W.M., Peng, B.X., 2008. Arc-like volcanic rocks from the southern Lancangjiang zone, SW China: gochronological and geochemical constraints on their petrogenesis and tectonic implications. Lithos 102, 358-373.

Qi, X.X., Zeng, L.S., Zhu, L.H., Hu, Z.C., Hou, K.J., 2012. Zircon U-Pb and Lu-Hf isotopic systematics of the Daping plutonic rocks: Implications for the Neoproterozoic tectonic evolution of the northeastern margin of the Indochina Bock, Southwest China. Gondwana Research 21, 180-193

Qi, X.X., Zhao, Y.H., Zhu, L.H., Li, Z.Q., 2012. Discovery of high-pressure pelitic granulite in Ailaoshan orogenic belt, southeastern Tibet, and its tectonic implications. Acta Petrologica Sinica 28, 1846-1856 (in Chinese with English abstract).

Rapp, R.P., Shimizu, N., Norman, M.D., 2003. Growth of early continental crust by partial melting of eclogite. Nature 425, 605-609.

Rapp, R.P., Watson, E.B., 1995. Dehydration melting of metabasalt at 8-32-kbar-implications for continental growth and crust-mantle recycling. Journal of Petrology 36, 891-931.

Roger, F., Maluski, H., Lepvrier, C., Van, T.V., Paquette, J.L., 2012. LA-ICPMS zircons U/Pb dating of Permo-Triassic and Cretaceous magmatisms in Northern Vietnam and godynamical implications. Journal of Asian Earth Sciences 48, 72-82.

Roger, F., Maluski, H., Leyreloup, A., Lepvrier, C., Thi, P.T., 2007. U-Pb dating of high temperature metamorphic episodes in the Kon Tum Massif (Vietnam). Journal of Asian Earth Sciences 30, 565-572.

Rudnick, R.L., Fountain, D.M., 1995. Nature and composition of the continental crust - a lower crustal perspective. Reviews of Geophysics 33, 267-309.

Searle, M.P., Yeh, M.W., Lin, T.H., Chung, S.L., 2010. Structural constraints on the timing of left-lateral shear along the Red River shear zone in the Ailao Shan and Diancang Shan Ranges, Yunnan, SW China. Geosphere 6, 316-338.

Shen, S.Y., Wei, Q.R., Cheng, H.L., Mo, X.X., 1998. Metamorphic peridotite and rock series of ophiolite belt in Mt. Ailao, Yunnan Province. Chinese Science Bulletin 43, 955-958.

Soderlund, U., Patchett, J.P., Vervoort, J.D., Isachsen, C.E., 2004. The Lu-176 decay constant determined by Lu-Hf and U-Pb isotope systematics of Precambrian mafic intrusions. Earth and Planetary Science Letters 219, 311-324.

Streule, M.J., Searle, M.P., Waters, D.J., Horstwood, M.S.A., 2010. Metamorphism, melting, and channel flow in the Greater Himalayan Sequence and Makalu leucogranite: constraints from thermobarometry, metamorphic modeling, and U-Pb geochronology. Tectonics 29, 1-28.

Sun, S.S., McDonough, W.F., 1989. Chemical and isotopic systematics of oceanic basalts: implication for mantle composition and process. Geological Society, London, Special Publications 42, 313-345.

Sylvester, P.J., 1998. Postcollisional strongly peraluminous granites. Lithos 45, 29-44.

Tang, L.M., Chen, H.L., Dong, C.W., Yang, S.F., Shen, Z.Y., Cheng, X.G., Fu, L.L., 2013a. Middle Triassic post-orogenic extension on Hainan Island: chronology and geochemistry constraints of bimodal intrusive rocks. Science China-Earth Sciences 56, 783-793.

Tang, Y., Liu, J.L., Tran, M.D., Song, Z.J., Wu, W.B., Zhang, Z.C., Zhao, Z.D., Chen, W., 2013b. Timing of left-lateral shearing along the Ailao Shan-Red River shear zone: constraints from zircon U-Pb ages from granitic rocks in the shear zone along the Ailao Shan Range, Western Yunnan, China. International Journal of Earth Sciences 102, 605-626.

Tapponnier, P., Lacassin, R., Leloup, P.H., Scharer, U., Zhong, D.L., Wu, H.W., Liu, X.H., Ji, S.C., Zhang, L.S., Zhong, J.Y., 1990. The Ailao Shan-Red River metamorphic belt - Tertiary left lateralshear between Indochina and South China. Nature 343, 431-437.

Taylor, S.R., McLennan, S.M., 1985. The continental crust:its composition and evolution. Oxford Press, Blackwell, 1-312.

Thompson, A.B., Connolly, J.A.D., 1995. Melting of the continental crust - some thermal and petrological constraints on anatexis in continental collision zones and other tectonic settings. Journal of Geophysical Research-Solid Earth 100, 15565-15579.

Wang, B.D., Wang, L.Q., Wang, D.B., Zhang, W.P., 2011. Zircons U-Pb dating of volcanic rocks from Renzhixueshan Formation in Shangdie rift basin of Sanjiang area and its geological implications. Acta Petrologica et Mineralogica 30, 25-33（in Chinese with English abstract）.

Wang, X.F., Metcalfe, I., Jian, P., He, L.Q., Wang, C.S., 2000. The Jinshajiang-Ailaoshan Suture Zone, China: tectonostratigraphy, age and evolution. Journal of Asian Earth Sciences 18, 675-690.

Wang, Y.J., Fan, W.M., Sun, M., Liang, X.Q., Zhang, Y.H., Peng, T.P., 2007. Geochronological, geochemical and geothermal constraints on petrogenesis of the Indosinian peraluminous granites in the South China Block: A case study in the Hunan Province. Lithos 96, 475-502.

Wang, Y.J., Fan, W.M., Zhang, G.W., Zhang, Y.H., 2013. Phanerozoic tectonics of the South China Block: Key observations and controversies. Gondwana Research 23, 1273-1305.

Wang, Y.J., Zhang, A.M., Fan, W.M., Peng, T.P., Zhang, F.F., Zhang, Y.H., Bi, X.W., 2010. Petrogenesis of late Triassic post-collisional basaltic rocks of the Lancangjiang tectonic zone, southwest China, and tectonic implications for the evolution of the eastern Paleotethys Geochronological and geochemical constraints. Lithos 120, 529-546.

Wen, S.N., 2013. Geochronological and geochemical studies of Permian-Triassic magmatism in Hainan Island, South China. Doctor dissertation, Beijing: University of Chinese Academy of Scienses (in Chinese).

Wu, F.Y., Yang, Y.H., Xie, L.W., Yang, J.H., Xu, P., 2006. Hf isotopic compositions of the standard zircons and baddeleyites used in U-Pb geochronology. Chemical Geology 234, 105-126.

Xie, C.F., Zhu, J.C., Ding, S.J., Zhang, Y.M., Chen, M.L., Fu, Y.R., Fu, T.A., Li, Z.H., 2006. Age and petrogenesis of the Jianfengling granite and its relationship to metallogenesis of the Baolun gold deposit, Hainan Island. Acta Petrologica Sinica 22, 2493-2508 (in English with Chinese abstract).

Xu, J.F., Castillo, P.R., 2004. Geochemical and Nd-Pb isotopic characteristics of the Tethyan asthenosphere: implications for the origin of the Indian Ocean mantle domain. Tectonophysics 393, 9-27.

Yang, J.H., Wu, F.Y., Shao, J.A., Wilde, S.A., Xie, L.W., Liu, X.M., 2006. Constraints on the timing of uplift of the Yanshan Fold and Thrust Belt, North China. Earth and Planetary Science Letters 246, 336-352.

Yang, X.A., Liu, J.J., Li, D.P., Zhai, D.G., Yang, L.B., Han, S.Y., Wang, H., 2013. Zircon U-Pb dating and geochemistry of the Linong granitoid and its relationship to Cu mineralization in the Yangla copper deposit, Yunnan, China. Resource Geology 63, 224-238.

Yang, Y.H., Zhang, H.F., Xie, L.W., Wu, F.Y., 2007. Accurate measurement of neodymium isotopic composition using Neptune Multiple Collector Inductively Coupled Plasma Mass Spectrometry. Chinese Journal of Analytical Chemistry 1, 71-74 (in Chinese with English abstract).

Yuan, H.L., Gao, S., Liu, X.M., Li, H.M., Gunther, D., Wu, F.Y., 2004. Accurate U-Pb age and trace element determinations of zircon by laser ablation-inductively coupled plasma-mass spectrometry. Geostandards and Geoanalytical Research 28, 353-370.

Yunnan BGMR, 1990. Regional geology of Yunnan Province. Beijing: Geology Publishing House, 273-428 (in Chinese).

Zen, E.A., 1986. Aluminum enrichment in silicate melts by fractional crystallization - some

mineralogic and petrographic constraints. Journal of Petrology 27, 1095-1117.

Zhang, F.F., Wang, Y.J., Chen, X.Y., Fan, W.M., Zhang, Y.H., Zhang, G.W., Zhang, A.M., 2011. Triassic high-strain shear zones in Hainan Island (South China) and their implications on the amalgamation of the Indochina and South China Blocks: Kinematic and Ar^{40}/Ar^{39} geochronological constraints. Gondwana Research 19, 910-925.

Zhang, H.F., Harris, N., Parrish, R., Kelley, S., Zhang, L., Rogers, N., Argles, T., King, J., 2004. Causes and consequences of protracted melting of the mid-crust exposed in the North Himalayan antiform. Earth and Planetary Science Letters 228, 195-212.

Zhong, D.L., 2000. The Paleotethysides in West Yunnan and Sichuan. Beijing: Science Press, 1-230 (in Chinese).

Zhu, D.C., Zhao, Z.D., Niu, Y.L., Dilek, Y., Hou, Z.Q., Mo, X.X., 2013. The origin and pre-Cenozoic evolution of the Tibetan Plateau. Gondwana Research 23, 1429-1454.

Zhu, J.J., Hu, R.Z., Bi, X.W., Zhong, H., Chen, H., 2011. Zircon U-Pb ages, Hf-O isotopes and whole-rock Sr-Nd-Pb isotopic geochemistry of granitoids in the Jinshajiang suture zone, SW China: Constraints on petrogenesis and tectonic evolution of the Paleo-Tethys Ocean. Lithos 126, 248-264.

Zi, J.W., Cawood, P.A., Fan, W.M., Tohver, E., Wang, Y.J., McCuaig, T.C., 2012a. Generation of Early Indosinian enriched mantle-derived granitoid pluton in the Sanjiang Orogen (SW China) in response to closure of the Paleo-Tethys. Lithos 140, 166-182.

Zi, J.W., Cawood, P.A., Fan, W.M., Tohver, E., Wang, Y.J., McCuaig, T.C., Peng, T.P., 2013. Late Permian-Triassic magmatic evolution in the Jinshajiang orogenic belt, SW China and implications for orogenic processes following closure of the Paleo-Tethys. American Journal of Science 313, 81-112.

Zi, J.W., Cawood, P.A., Fan, W.M., Wang, Y.J., Tohver, E., 2012b. Contrasting rift and subduction-related plagiogranites in the Jinshajiang ophiolitic melange, southwest China, and implications for the Paleo-Tethys. Tectonics 31, 1-18.

Zi, J.W., Cawood, P.A., Fan, W.M., Wang, Y.J., Tohver, E., McCuaig, T.C., Peng, T.P., 2012c. Triassic collision in the Paleo-Tethys Ocean constrained by volcanic activity in SW China. Lithos 144, 145-160.

Figure captions

Fig. 1 (a) Tectonic outline of Southeast Asia (after Wang et al., 2010). The Jinshajiang Suture, Ailaoshan Suture, Song Ma Suture and Hainan Suture are considered to be contiguous and mark the boundaries between the Simao-Indochina Block and the South China Craton. (b) Geological map showing the stratigraphic and igneous components of the Ailaoshan area (after Yunnan BGMR, 1990).

Fig. 2 (a-b) Cathodoluminescence (CL) images of representative zircon grains. Red circles on CL images mark analytical site on each grain and number in circle denotes spots number. (c-f) LA-ICP-MS zircon U-Pb concordia diagrams for the Xin'anzhai monzogranites (c and e) and Tongtiange leucogranites (d and f).

Fig. 3 Zircon $\varepsilon_{Hf}(t)$ versus the emplacement ages of the Xin'anzhai and Tongtiange plutons in the Ailaoshan suture zone. The evolutionary line of depleted mantle is drawn after Zi et al. (2012a). The lines of crustal extraction are calculated by assuming the $^{176}Lu/^{177}Hf$ ratio of 0.015 for the average continental crust after Griffin et al. (2002).

Fig. 4 (a) A/CNK versus A/NK; (b) SiO_2 versus MgO+FeOt+TiO_2; (c-j) Harker diagrams for for the Xin'anzhai monzogranites and Tongtiange leucogranites in the Ailaoshan suture zone. Symbols are the same as in Fig. 3.

Fig. 5 SiO_2 versus Sr (a), Ba (b), Eu (c), Zr (d), Nb (e) and La (f) for the Xin'anzhai monzogranites and Tongtiange leucogranites in the Ailaoshan suture zone. Symbols are the same as in Fig. 3.

Fig. 6 (a) Chondrite normalized REE patterns and (b) primitive mantle normalized incompatible elemental spidergrams for the Xin'anzhai monzogranites and Tongtiange leucogranites in the

Ailaoshan suture zone. Normalized values for primitive mantle and chondrite are from Sun and McDonough (1989).

Fig. 7 (a) $^{87}Sr/^{86}Sr(t)$ versus $\varepsilon_{Nd}(t)$ for the Xin'anzhai pluton in the Ailaoshan suture zone. The number marked on the mixing curves notes mass fractions (%) of the mafic component in the mixed source. Sr (ppm), Nd (ppm), $^{87}Sr/^{86}Sr(i)$ and $\varepsilon_{Nd}(t)$ for the end-members used in mixing calculation are 229.4, 23.6, 0.708581 and -0.27 for the Proterozoic amphibolite (authors' unpublished data), 141.9, 33.2, 0.723649 and -13.17 for Proterozoic gneiss (authors' unpublished data) and 350.0, 13.0, 0.704988 and 4.50 for the volcanic arc basalts (Fan et al., 2010), respectively. (b) Zr/Hf versus ε_{Nd} (t) for the Xin'anzhai monzogranites and Tongtiange leucogranites in the Ailaoshan suture zone. t=250 Ma. Symbols are the same as in Fig. 4.

Fig.8 (a) Rb/Ba versus Rb/Sr; (b) $CaO/(MgO+FeOt+TiO_2)$ versus $CaO+MgO+FeOt+TiO_2$; (c) CaO/Na_2O versus Al_2O_3/TiO_2; (d) $Al_2O_3/(FeOt+MgO+TiO_2)$ versus $Al_2O_3+FeOt+MgO+TiO_2$; (e) molar $Al_2O_3/(MgO+FeOt)$ versus molar $CaO/(MgO+FeOt)$; (f) $(Na_2O+K_2O)/(FeOt+MgO+TiO_2)$ versus $Na_2O+K_2O+FeOt+MgO+TiO_2$. (g) Ce/Pb versus Ce (ppm); (h) Nb/U versus Nb (ppm). Fields in (a-f) are from Patiño-Douce and Harris (1998), Sylvester (1998) and Patiño-Douce (1999). Data for MORB and OIB are taken from Sun and McDonough (1989). Data for Upper Continental Crust (UCC) and Bulk Continental Crust (BCC) are from Taylor and McLennan (1985) and Rudnick and Fountain (1995), respectively. Symbols are the same as in Fig. 4.

Fig. 9 Rb/Sr versus Ba for the Xin'anzhai and Tongtiange plutons in the Ailaoshan suture zone. Data for the Cambrian gneiss of the Northern Himalaya, North Himalayan granites and Himalayan leuogranites are from Inger and Harris (1993) and Zhang et al. (2004). The trends for dehydration muscovite and biotite melting and plagioclase fractional crystallization are from Inger and Harris

(1993), Zhang et al. (2004) and Streule et al. (2010). Symbols are the same as in Fig. 4.

Fig. 10 Compilation of age data associated with Tethyan ocean closure and Indosinian collision along the Jinshajiang-Ailaoshan-Song Ma-Hainan suture zone. The numerical and stage time scales are those of Gradstein et al. (2004). The timing of the late-Triassic unconformity is after Zi et al. (2013). Numbers on data points refer to the following sources: 1 Carter et al. (2001), 2 Lepvrier et al. (2004), 3 Lepvrier et al. (1997), 4 Zi et al. (2012a), 5 Liu et al. (2012), 6 Wen (2013), 7 Xie et al. (2006), 8 this study, 9 Liu et al. (2010), 10 Zi et al. (2012c), 11 Wang et al. (2011), 12 Zi et al. (2012c), 13 Searle et al. (2010), 14 Lin et al. (2012), 15 Nakano et al. (2010), 16 Zhang et al. (2011), 17 Zhu et al. (2011), 18 Jian et al. (2003), 19 Zi et al. (2013), 20 Gao et al. (2010), 21 Yang et al. (2013), 22 Tang et al. (2013a), 23 Nakano et al. (2008), 24 Liu et al. (in press), 25 Lai et al. (in press).

Fig. 11 Temporal distribution of magmatic activities in SW Yunnan and relations with major tectonic events during late Paleozoic and early Mesozoic. Numbers on data points refer to the following sources: 1 Jian et al. (2009b), 2 Zhong (2000), 3 Wang et al. (2000), 4 Fan et al. (2010), 5 Zi et al. (2012b), 6 Li et al. (2012), 7 Liu et al. (2012), 8 Liu et al. (2011), 9 Zi et al. (2012a), 10 Zi et al. (2012c), 11 Wang et al. (2011), 12 Liu et al. (in press), 13 Peng et al. (2008), 14 Zi et al. (2013), 15 this study, 16 Lai et al. (in press).

Table captions

Table 1 Summary of lithology, zircon U-Pb age and Hf-Nd isotopes of the representative samples from Xin'anzhai and Tongtiange plutons.

Table 2 Major oxide (wt %), trace (ppm) element and Sr-Nd isotopic composition for the Tongtiange and Xin'anzhai granites in the Ailaoshan suture zone

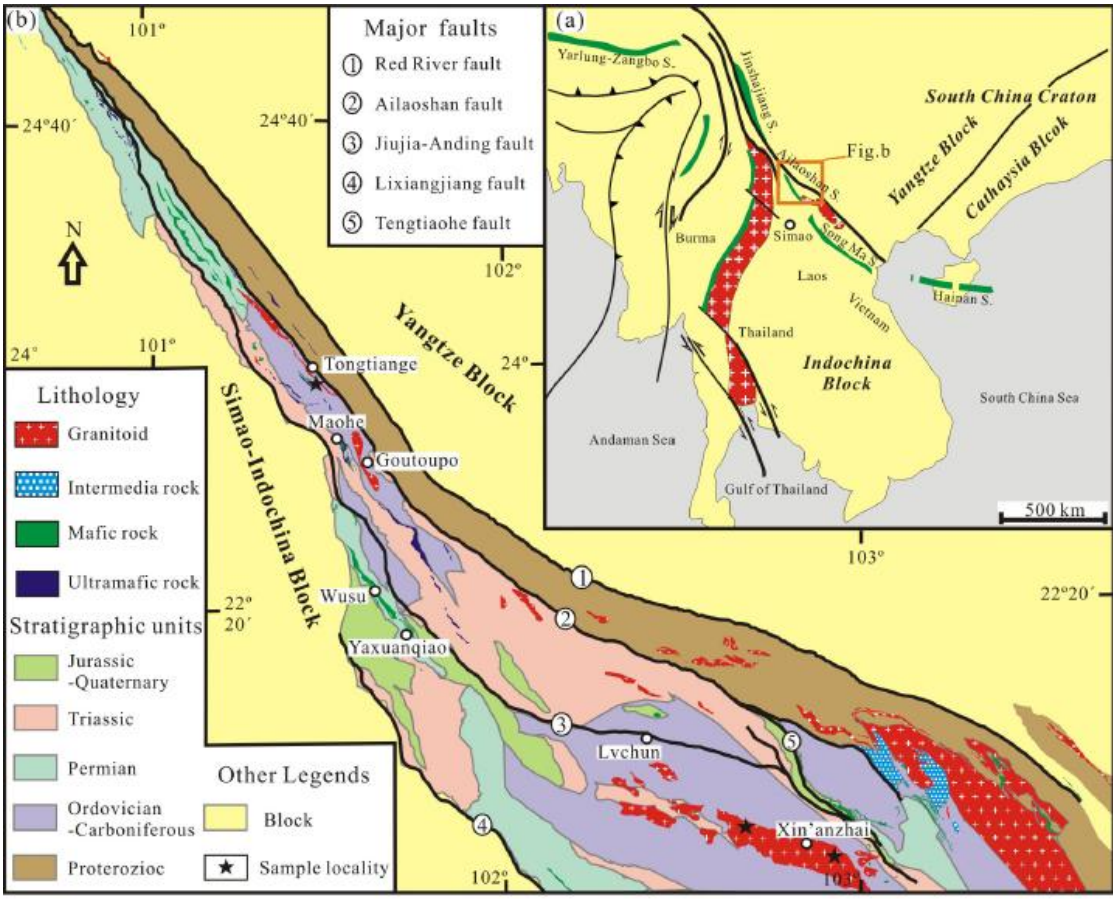

Fig. 1 H-C Liu & coauthors

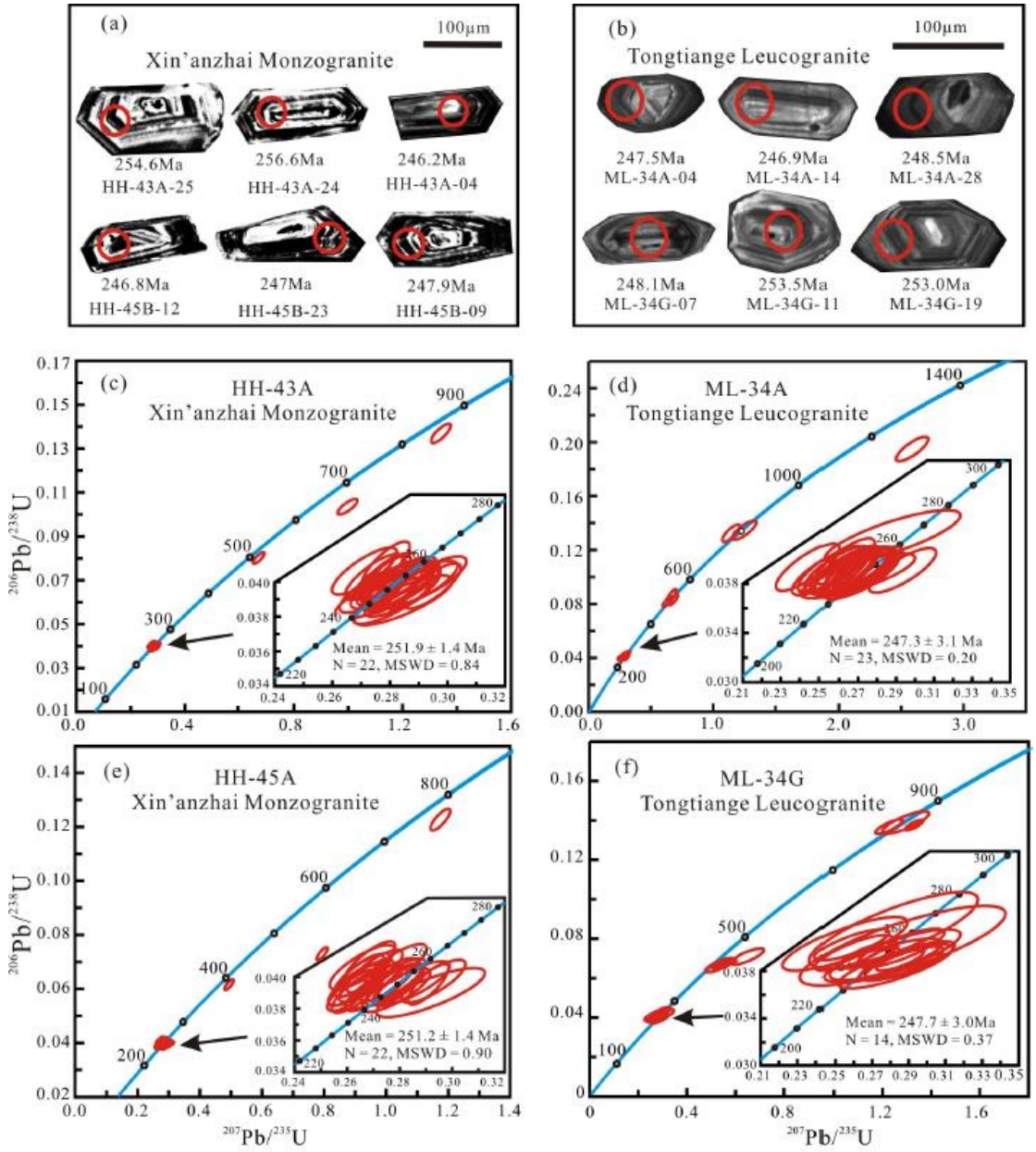

Fig. 2 H-C Liu & coauthors

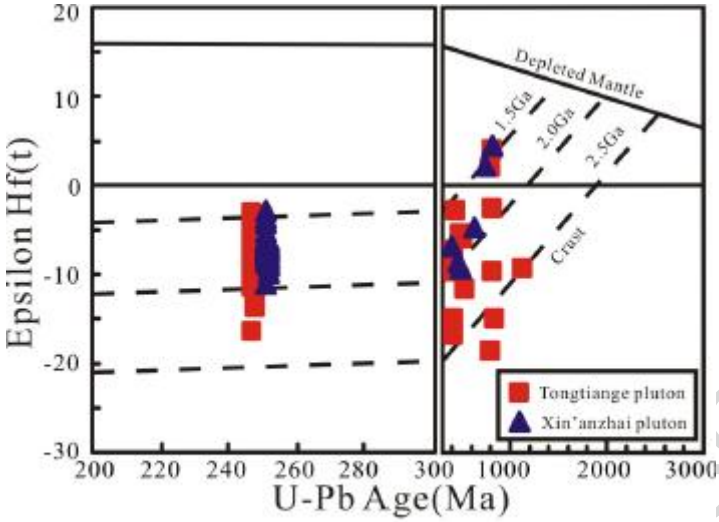

Fig. 3 H-C Liu & coauthors

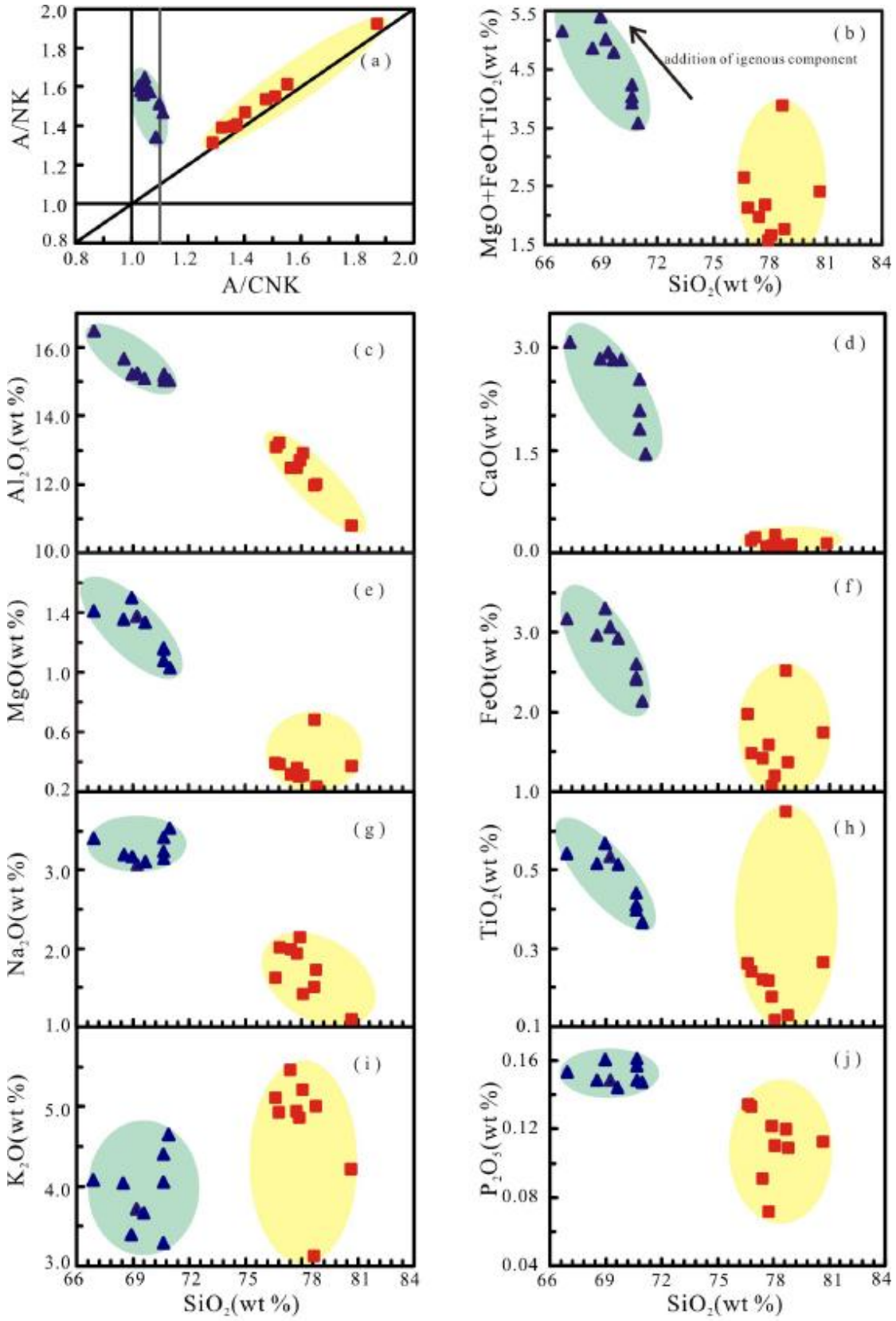

Fig. 4 H-C Liu & coauthors

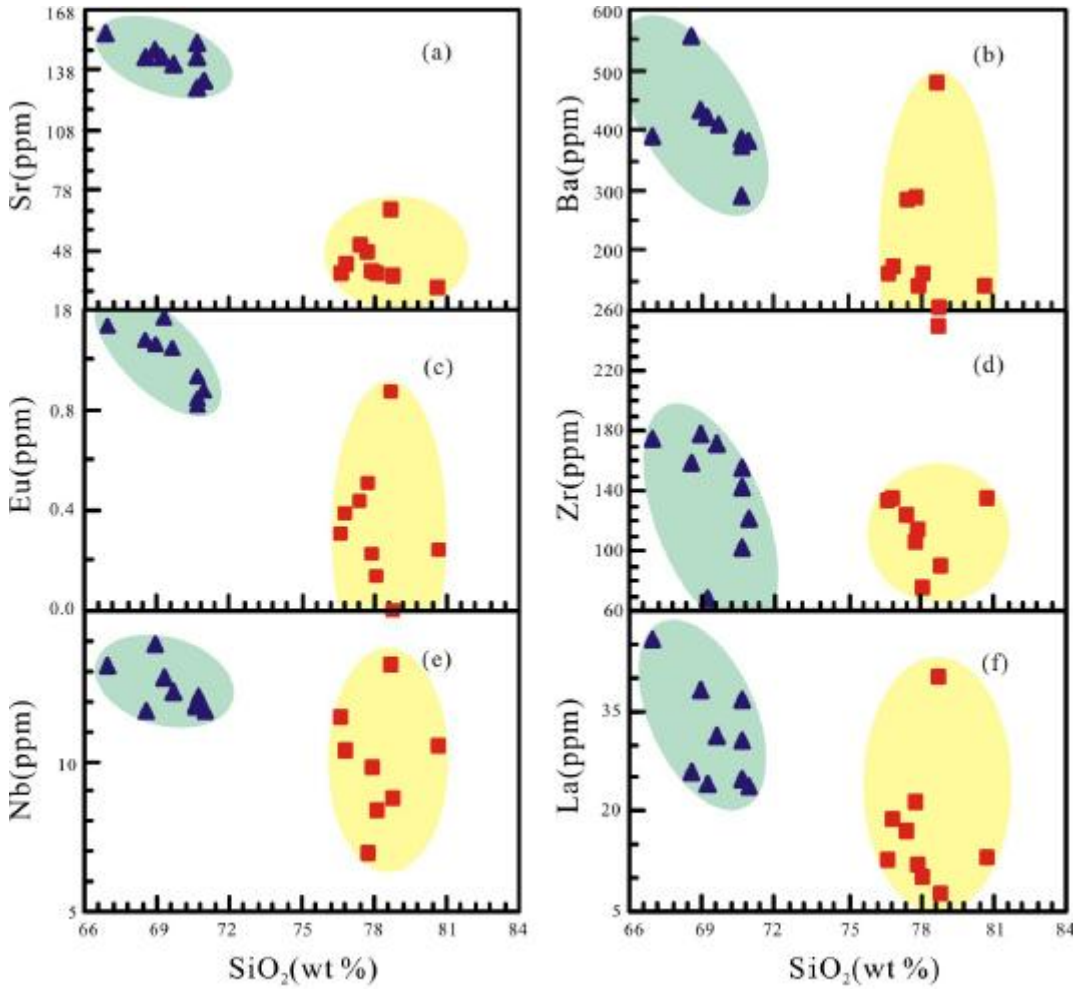

Fig. 5 H-C Liu & coauthors

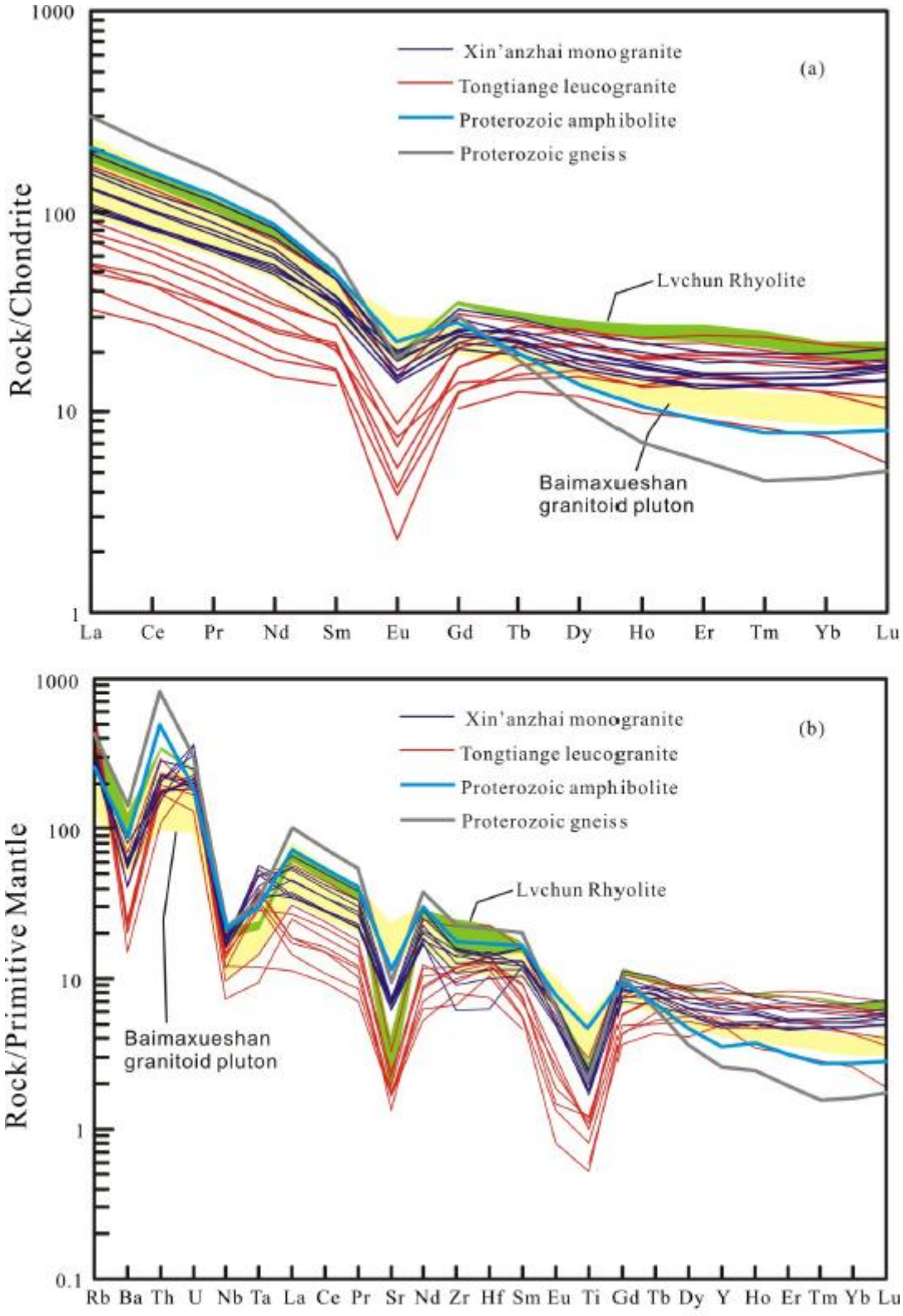

Fig. 6 H-C Liu & coauthors

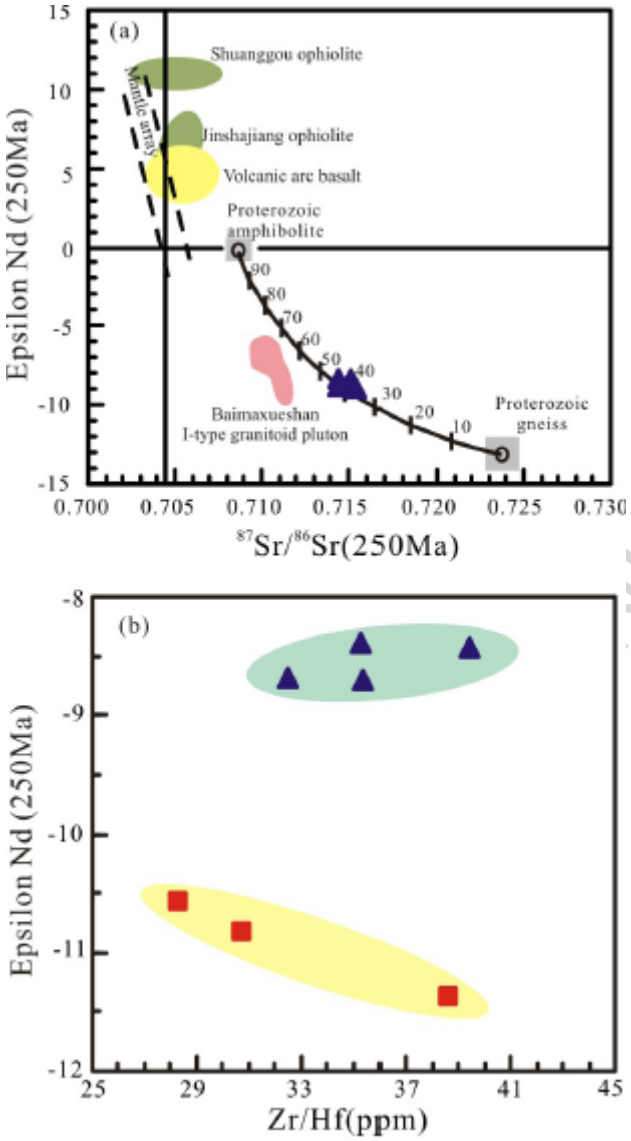

Fig. 7 H-C Liu & coauthors

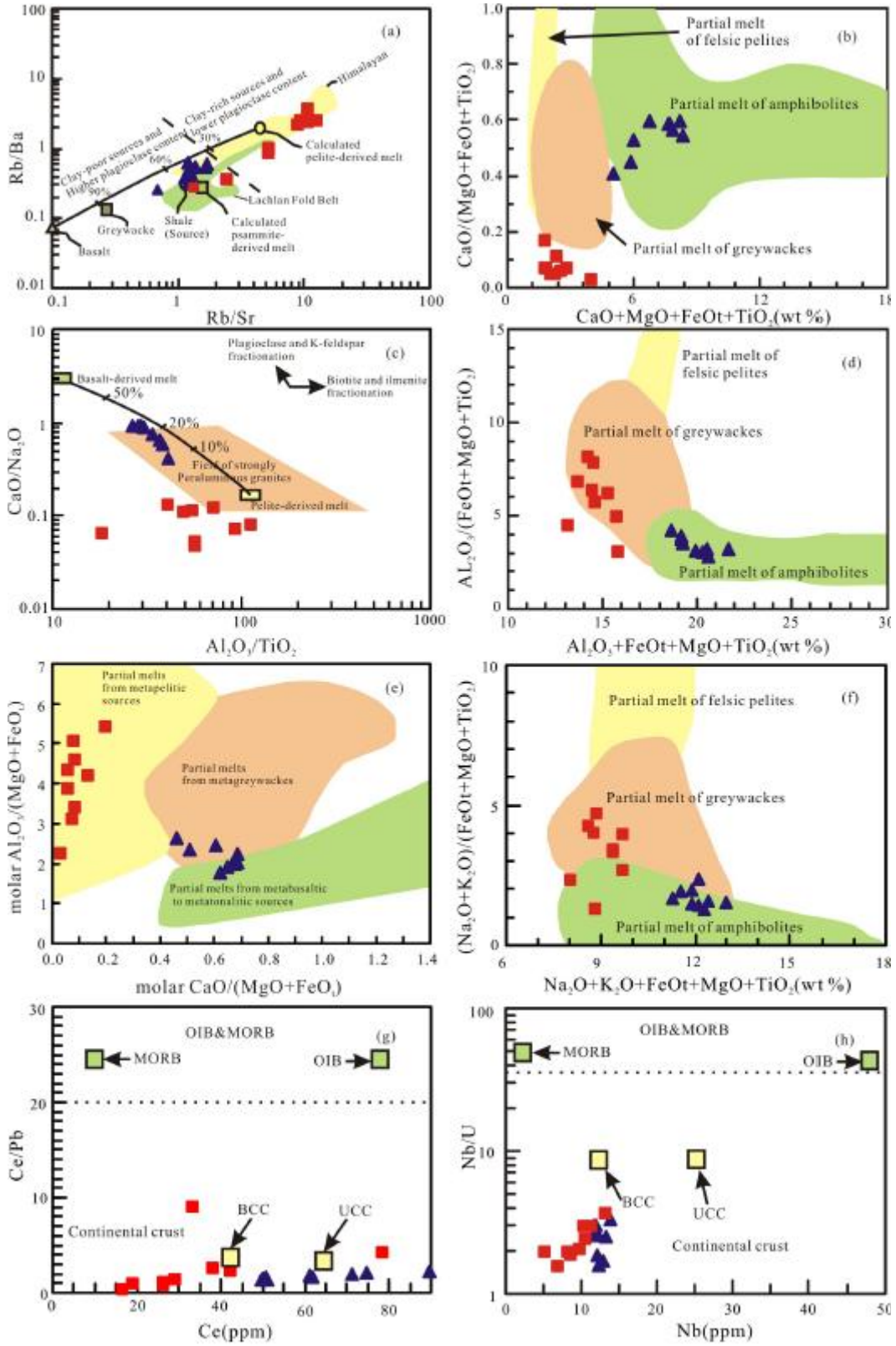

Fig. 8 H-C Liu & coauthors

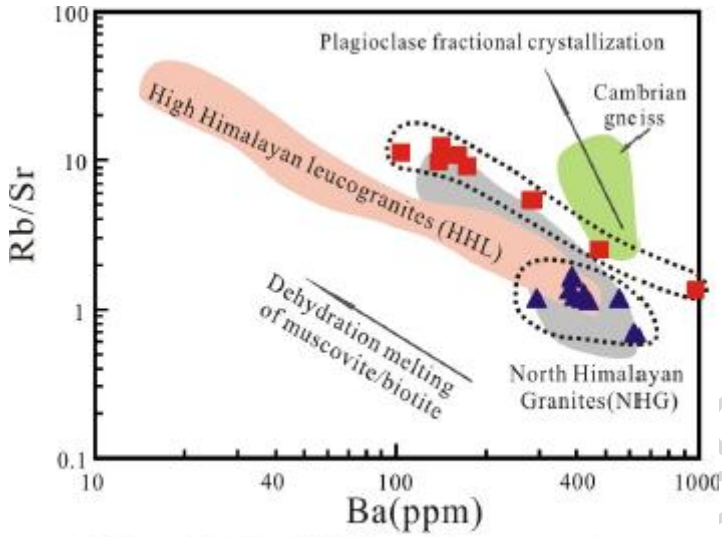

Fig. 9 H-C Liu & coauthors

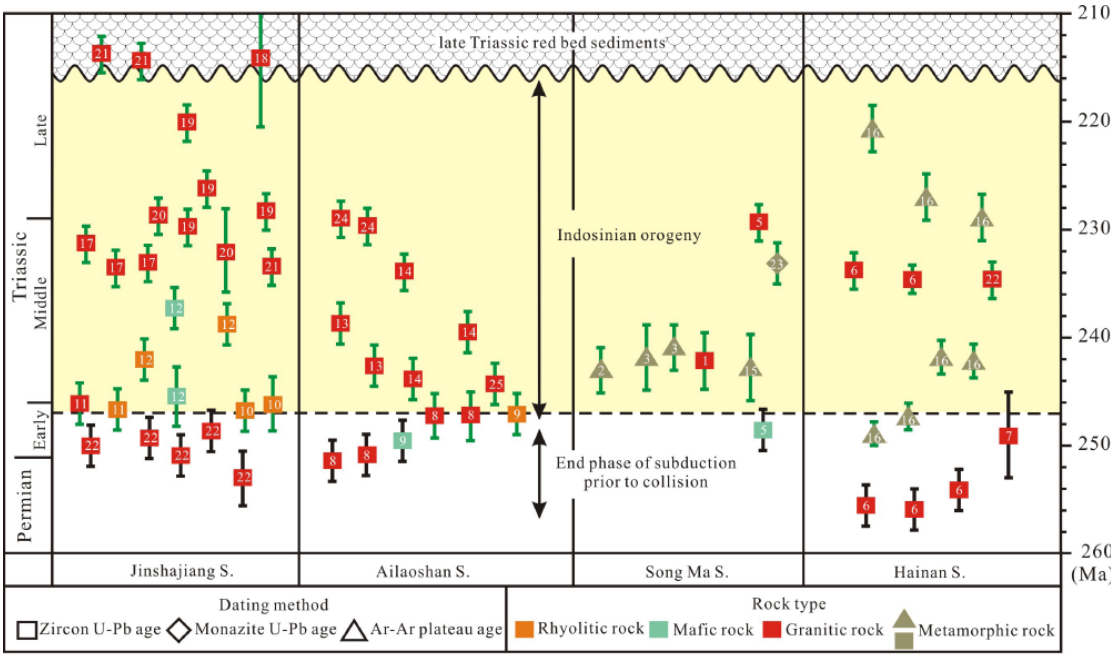

Fig. 10 H-C Liu & Coauthors

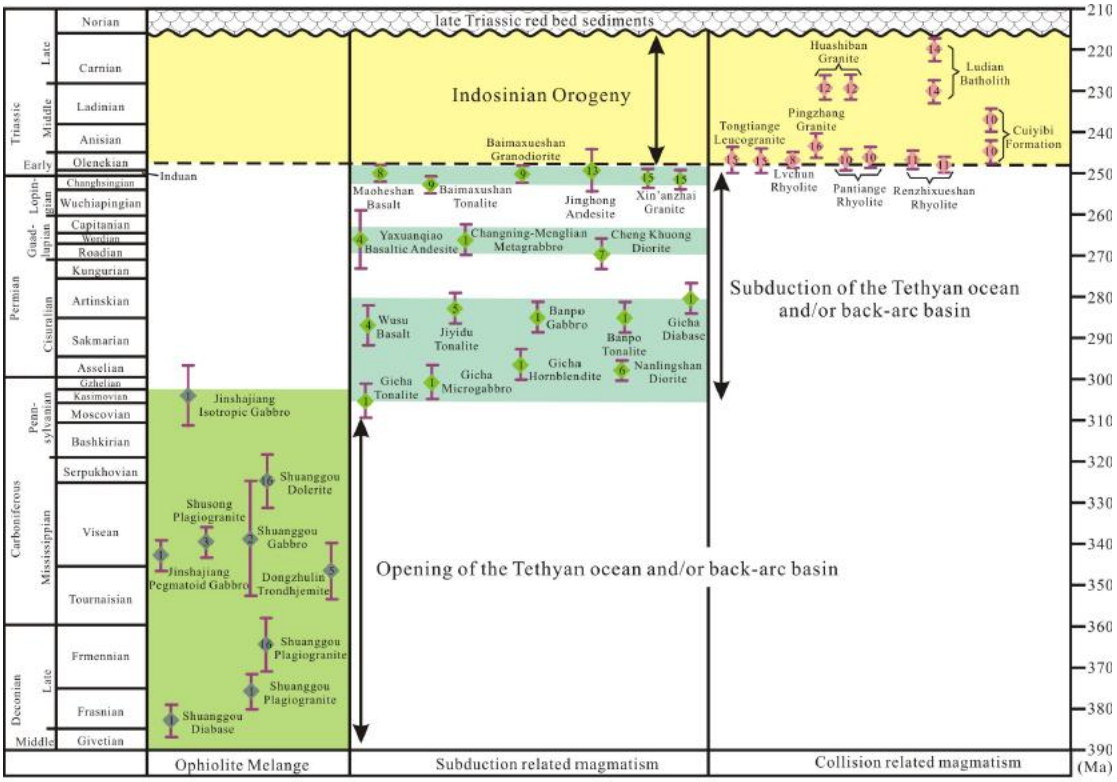

Fig. 11 H-C Liu & coauthors

Table 1 Summary of lithology, zircon U-Pb age and Hf-Nd isotopes of the representative samples from Xin'anzhai and Tongtiange plutons.

Sample	Pluton	Rock type	Location	Age (Ma)	$\varepsilon_{Hf}(t)$	$\varepsilon_{Nd}(t)$	SiO_2 (wt %)	A/CNK
HH-43A	Xin'anzhai	Monzogranite	N 22°42′28.6″ E102°53′59.5″	251.9 ± 1.4	-9.8 ~ -6.2	-8.8	68.80	1.05
HH-43C							66.57	1.03
HH-43D						-8.5	68.04	1.03
HH-43E							69.27	1.04
HH-43F							68.43	1.05
HH-45A	Xin'anzhai	Monzogranite	N 22°45′36.8″ E102°43′52.4″	251.2 ± 1.4	-11.1 ~ -3.1	-8.5	70.02	1.10
HH-45B							69.92	1.09
HH-45D						-8.8	69.98	1.12
HH-45E							69.99	1.06
ML-34A	Tongtiange	Leucogranite	N 23°56′36.4″ E101°30′03.4″	247.3 ± 3.1	-16.6 ~ -3.2	-10.8	75.48	1.48
ML-34B							79.55	1.55
ML-34C							76.76	1.87
ML-34D						-10.6	76.61	1.38
ML-34E							76.99	1.32
ML-34F							75.95	1.40
ML-34G	Tongtiange	Leucogranite	N 23°56′24.0″ E101°29′56.2″	247.7 ± 3.0	-11.9 ~ -3.4	-11.4	77.75	1.36
ML-34H							76.92	1.51
ML-34I							76.19	1.29

Table 2 Major oxide (wt. %), trace (ppm) element and Sr-Nd isotopic composition for the Tongtiange and Xin'anzhai granites in the Ailaoshan suture zone

Sample	Xin'anzhai granite									Tongtiange granite								
	HH -43A	HH -43C	HH -43D	HH -43E	HH -43F	HH -45A	HH -45B	HH -45D	HH -45E	ML -34A	ML -34B	ML -34C	ML -34D	ML -34E	ML -34F	ML -34G	ML -34H	ML -34I
SiO_2	68.80	66.57	68.04	69.27	68.43	70.02	69.92	69.98	69.99	75.48	79.55	76.76	76.61	76.99	75.95	77.75	76.92	76.19
TiO_2	0.53	0.54	0.51	0.51	0.56	0.41	0.36	0.39	0.44	0.26	0.26	0.63	0.21	0.17	0.24	0.13	0.11	0.21
Al_2O_3	15.15	16.40	15.56	15.02	15.11	15.09	14.82	15.01	14.89	12.88	10.64	11.65	12.27	12.53	13.05	11.82	12.69	12.26
FeOt	3.39	3.51	3.27	3.23	3.65	2.65	2.35	2.68	2.87	2.15	1.91	2.72	1.73	1.16	1.62	1.49	1.31	1.54
MnO	0.05	0.05	0.05	0.05	0.05	0.05	0.05	0.05	0.05	0.03	0.01	0.00	0.01	0.01	0.01	0.01	0.01	0.01
MgO	1.40	1.44	1.37	1.36	1.52	1.10	1.05	1.18	1.17	0.41	0.39	0.69	0.38	0.33	0.41	0.26	0.33	0.34
CaO	2.81	3.06	2.82	2.81	2.91	2.06	1.43	1.80	2.50	0.17	0.14	0.09	0.10	0.26	0.23	0.12	0.11	0.09
Na_2O	3.05	3.39	3.17	3.09	3.15	3.21	3.48	3.11	3.39	1.59	1.07	1.46	1.90	2.11	1.99	1.70	1.40	1.95
K_2O	4.02	4.39	4.34	3.98	3.69	4.34	4.91	4.68	3.59	5.34	4.47	3.37	5.19	5.13	5.19	5.25	5.45	5.68
P_2O_5	0.15	0.15	0.15	0.14	0.16	0.16	0.15	0.16	0.15	0.13	0.11	0.12	0.07	0.12	0.13	0.11	0.11	0.09
L.O.I	0.75	0.62	0.80	0.64	0.87	1.01	1.60	1.05	1.07	1.48	1.23	2.08	1.12	1.17	1.17	1.26	1.48	1.23
Total	100.08	100.11	100.09	100.09	100.09	100.10	100.12	100.10	100.12	99.93	99.78	99.58	99.59	99.98	99.98	99.90	99.94	99.58
A/CNK	1.05	1.03	1.03	1.04	1.05	1.10	1.09	1.12	1.06	1.48	1.55	1.87	1.38	1.32	1.40	1.36	1.51	1.29
Sc	8.08	8.42	7.38	7.58	8.81	8.14	7.56	8.15	8.89	4.53	3.13	8.20	4.67	4.39	5.52	2.98	3.85	3.87
V	45.2	47.2	42.7	44.2	50.9	35.0	30.7	33.4	38.1	13.6	12.9	39.5	13.7	12.4	14.1	5.5	4.2	12.7
Cr	113	8.52	18.3	24.8	28.9	7.49	1.58	9.79	7.39	9.30	13.9	27.0	10.9	11.8	8.43	2.63	6.88	10.1
Co	8.65	7.50	7.51	6.91	8.37	5.92	5.03	5.04	6.11	1.83	1.87	1.58	1.62	0.99	1.76	0.89	1.03	0.93
Ni	82.24	5.44	10.88	8.76	11.37	4.51	3.43	4.10	7.54	5.54	7.51	11.12	8.95	5.62	4.52		5.21	5.36
Ga	17.3	18.2	16.7	16.2	17.8	16.3	15.8	16.3	16.8	15.9	15.0	13.6	13.6	15.2	16.6	13.5	13.1	13.2
Rb	183	191	174	171	169	199	228	212	181	381	352	169	245	352	368	377	388	264
Sr	144	156	144	141	148	144	133	129	152	35.3	28.1	68.0	46.3	36.8	40.8	34.5	35.6	49.9
Y	31.0	28.8	27.0	30.1	39.0	22.4	22.3	21.5	26.2	32.7	34.0	28.8	35.9	25.1	42.8	22.3	23.0	21.4

Sample	Xin'anzhai granite									Tongtiange granite								
	HH -43A	HH -43C	HH -43D	HH -43E	HH -43F	HH -45A	HH -45B	HH -45D	HH -45E	ML -34A	ML -34B	ML -34C	ML -34D	ML -34E	ML -34F	ML -34G	ML -34H	ML -34I
Zr	68.3	174	158	171	178	142	122	101	155	132	134	248	105	113	134	88.5	75.0	123
Nb	12.8	13.2	11.7	12.3	13.9	11.9	11.7	11.8	12.1	11.4	10.5	13.2	6.91	9.76	10.3	8.70	8.36	5.25
Cs	16.2	13.7	13.8	15.2	14.5	17.8	11.4	16.8	11.1	13.8	13.3	3.31	3.57	9.94	11.5	7.75	11.3	3.45
Ba	421	389	555	411	434	376	383	387	290	161	141	476	287	140	172	105	159	281
La	24.0	45.6	25.8	31.3	38.2	36.7	23.6	24.8	30.7	12.7	12.9	39.8	21.1	11.8	18.6	7.66	9.91	17.0
Ce	49.7	89.5	51.2	61.9	74.8	71.1	50.9	50.1	61.2	26.5	29.1	78.7	42.4	26.5	38.3	16.7	19.2	33.3
Pr	6.16	10.6	6.36	7.67	9.20	8.42	6.37	6.03	7.29	3.24	3.32	9.25	4.94	2.82	4.45	1.93	2.36	3.93
Nd	23.5	38.4	24.2	28.4	34.4	30.6	25.0	22.8	27.3	11.6	12.1	33.3	16.7	9.61	15.9	7.08	8.57	14.1
Sm	5.39	7.08	5.35	5.86	7.04	5.71	5.11	4.60	5.44	3.26	3.40	7.06	4.06	2.50	4.15	2.06	2.45	3.08
Eu	1.17	1.14	1.08	1.05	1.06	0.935	0.876	0.820	0.849	0.307	0.243	0.869	0.504	0.222	0.389		0.134	0.436
Gd	5.25	6.06	5.12	5.36	6.66	4.96	4.56	4.23	4.89	3.44	3.42	6.36	4.34	2.59	4.57	2.15	2.55	2.90
Tb	0.949	0.918	0.840	0.911	1.10	0.831	0.789	0.724	0.854	0.810	0.788	1.05	0.907	0.572	1.00	0.470	0.637	0.540
Dy	5.51	5.06	4.73	5.07	6.21	4.40	4.17	4.16	4.67	5.56	5.42	5.97	6.45	4.09	6.61	3.03	4.62	3.80
Ho	1.12	0.970	0.928	1.00	1.25	0.846	0.820	0.816	0.946	1.05	1.06	1.03	1.31	0.750	1.23	0.560	0.850	0.770
Er	2.90	2.45	2.45	2.57	3.29	2.23	2.16	2.24	2.53	3.16	3.32	3.07	3.99	2.28	3.63	1.53	2.46	2.52
Tm	0.459	0.378	0.373	0.399	0.495	0.348	0.344	0.352	0.400	0.480	0.480	0.440	0.600	0.340	0.520	0.210	0.360	0.380
Yb	2.92	2.57	2.52	2.71	3.31	2.34	2.30	2.35	2.70	3.03	3.13	2.78	3.69	2.14	3.16	1.27	2.11	2.50
Lu	0.462	0.414	0.401	0.422	0.527	0.366	0.366	0.360	0.437	0.424	0.445	0.435	0.519	0.297	0.424	0.140	0.265	0.360
Hf	1.93	4.29	4.01	4.21	4.47	4.02	3.56	3.12	4.66	4.29	4.39	6.97	3.71	3.55	3.97	2.29	3.21	3.94
Ta	1.50	1.51	1.39	1.45	1.68	1.98	2.01	2.19	2.30	1.55	1.64	2.03	0.590	1.34	1.17	0.490	1.27	0.39
Pb	38.4	40.0	38.5	39.4	35.5	37.8	31.7	34.1	33.9	26.6	21.3	19.0	18.4	38.0	14.9	46.0	19.9	3.71
Th	12.9	24.2	14.6	17.3	19.6	19.0	15.1	14.8	17.6	15.4	18.4	24.9	19.7	14.0	16.6	9.3	15.3	14.4
U	7.49	5.27	4.55	7.69	4.17	3.98	3.87	4.27	6.50	3.89	4.42	3.66	4.43	4.76	3.49	4.64	4.26	2.71
T_{Zr}(℃)	755	835	827	836	839	822	808	793	829	835	841	910	811	816	835	796	785	823

Sample	Xin'anzhai granite									Tongtiange granite								
	HH -43A	HH -43C	HH -43D	HH -43E	HH -43F	HH -45A	HH -45B	HH -45D	HH -45E	ML -34A	ML -34B	ML -34C	ML -34D	ML -34E	ML -34F	ML -34G	ML -34H	ML -34I
$^{87}Rb/^{86}Sr$	3.70		3.50			4.00		4.75		29.07			14.25			29.43		
$^{147}Sm/^{144}Nd$	0.138		0.134			0.113		0.122		0.170			0.147			0.176		
$^{87}Sr/^{86}Sr$	0.728081		0.727403			0.729864		0.732911										
2σ	0.000013		0.000011			0.000012		0.000013										
$^{143}Nd/^{144}Nd$	0.512093		0.512099			0.512065		0.512066		0.512038			0.512014			0.512020		
2σ	0.000006		0.000007			0.000006		0.000008		0.000026			0.000005			0.000013		
$(^{87}Sr/^{86}Sr)_i$	0.714931		0.714949			0.715651		0.716027										
$\varepsilon_{Nd}(t)$	-8.78		-8.50			-8.51		-8.78		-10.84			-10.59			-11.38		
$T_{DM}(Ga)$	2.14		2.00			1.64		1.80		3.82			2.59			4.50		

LOI: Loss ion ignition. Chondrite uniform reservoir values, $^{147}Sm/^{144}Nd=0.1967$ and $^{143}Nd/^{144}Nd=0.512638$, are used for the calculation. $\varepsilon_{Nd}(t)$ is calculated by assuming 250 Ma for these samples.

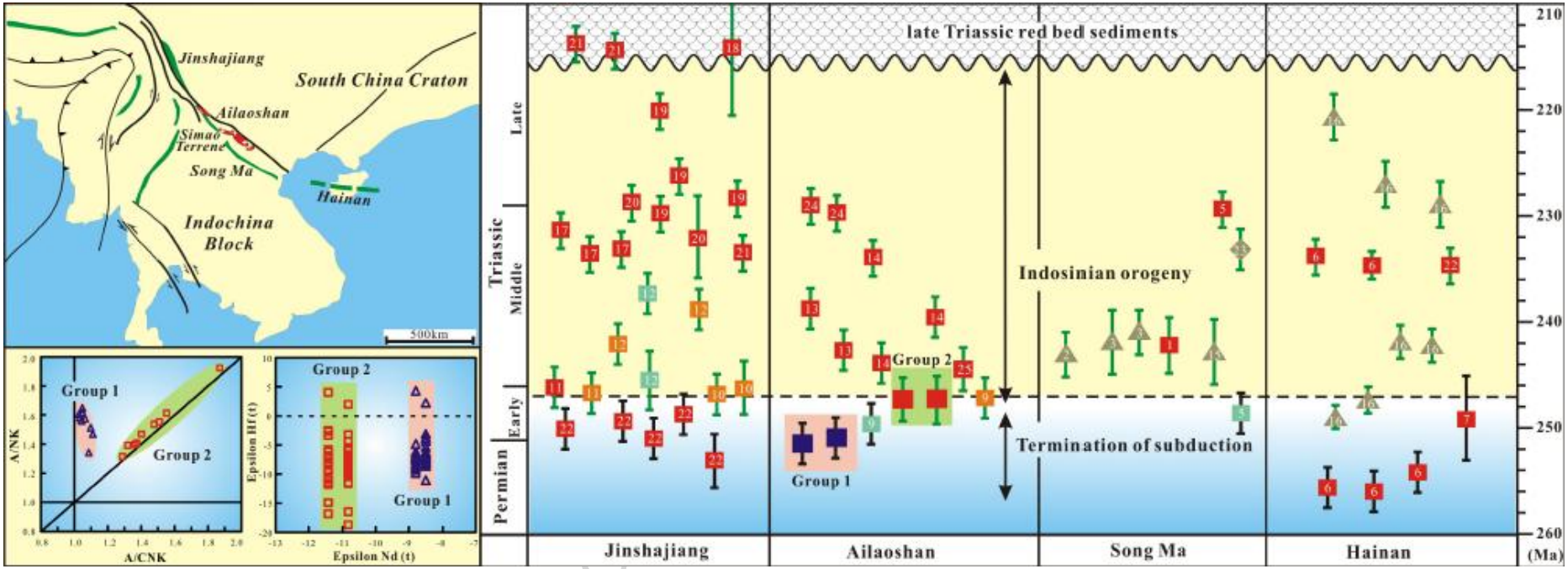

Graphical abstract

Highlights

► The granitic plutons in the Ailaoshan zone yield zircon U-Pb ages of 247-252 Ma.
► Indosinian magmatism were confirmed along the Ailaoshan zone
► The accretion of Indochina with South China Blocks occurred at ~247 Ma